MAX-PLANCK-INSTITUT FÜR PLASMAPHYSIK

GARCHING BEI MÜNCHEN

Three-Dimensional Computation of Drift-Alfvén Turbulence

Bruce Scott

IPP 5/74

April 1997

Die nachstehende Arbeit wurde im Rahmen des Vertrages zwischen dem Max-Planck-Institut für Plasmaphysik und der Europäischen Atomgemeinschaft über die Zusammenarbeit auf dem Gebiete der Plasmaphysik durchgeführt.

Three-Dimensional Computation of Drift Alfvén Turbulence

B. Scott

Max Planck Institut für Plasmaphysik
Euratom Association
D-85748 Garching, Germany

February 1997

Abstract

A transcollisional, electromagnetic fluid model, incorporating the parallel heat flux as a dependent variable, is constructed to treat electron drift turbulence in the regime of tokamak edge plasmas at the L-H transition. The resulting turbulence is very sensitive to the plasma beta throughout this regime, with the scaling with rising beta produced by the effect of magnetic induction to slow the Alfvénic parallel electron dynamics and thereby leave the turbulence in a more robust, nonadiabatic state. Magnetic flutter and curvature have a minor qualitative effect on the turbulence mode structure and on the beta scaling, even when their quantitative effect is strong. Transport by magnetic flutter is small compared to that by the ExB flow eddies. Fluctuation statistics show that while the turbulence shows no coherent structure, it is strongly enough coupled that neither density nor temperature fluctuations behave as passive scalars. Both profile gradients drive the turbulence, with the total thermal energy transport varying only weakly with the gradient ratio, d log T/d log n. Scaling with magnetic shear is pronounced, with stronger shear leading to lower drive levels. Scaling with either collision frequency or magnetic curvature is weak, consistent with their weak qualitative effect. The result is that electron drift turbulence at L-H transition edge parameters is drift Alfvén turbulence, with both ballooning and resistivity in a clear secondary role. The contents of the drift Alfvén model will form a significant part of any useful first-principles computation of tokamak edge turbulence.

PACS numbers:

52.35R—Plasma turbulence, 52.25F—Plasma transport properties, 52.65—Plasma simulation.

1. Introduction — Tokamak Edge Parameters

It has been often suspected that collisional electrostatic turbulence should play a central role in the process of anomalous transport in the tokamak edge, including in such phenomena as the L-H transition. The edge conditions are thought to be cold enough that the collision frequency is faster than the turbulence, and of low enough pressure that the magnetic activity associated with fluctuations in the plasma current — a natural feature of drift wave turbulence — is negligible, and the experiments appear to bear this out [1,2,3,4].

Years of intensive investigation via Langmuir probes into the dynamics of density (n), electron temperature (T_e, in units of energy), and electrostatic potential (ϕ) fluctuations in cold edge ($T_e < 50\,\mathrm{eV}$) regions of tokamaks and stellarators have shown a picture consistent with the interpretation that the fluctuations are of the drift wave type, with scales somewhat larger than the dispersion scale, $\rho_s = c\sqrt{M_i T_e}/eB$, a frequency range corresponding to the observed wavenumbers perpendicular to the mean magnetic field, $k_\perp \rho_s$, responding near their diamagnetic frequency, $\omega_*(k_\perp) = k_\perp \rho_s c_s / L_\perp$, where $c_s = \sqrt{T_e/M_i}$ is the sound speed and $L_\perp$ is the mean profile scale length across the magnetic flux surfaces of the mean field (all parameters are local to a given flux surface, where a given data point is taken, and subscripts 'e' and 'i' refer to electrons and ions, respectively) [5–12]. These scales are in the range 0.1 to 1 cm and 100 kHz to 1 MHz, with experimental spectrum peaks at the low end of these ranges. Typical values of the reference scales are $\rho_s \sim 0.5\,\mathrm{mm}$, $L_\perp \sim 2\,\mathrm{cm}$, and $c_s/L_\perp \sim 2\,\mathrm{MHz}$. In a few instances, magnetic fluctuations measured in the same scale ranges, assumed to be attendant to the other fluctuations, have been found to be too small to cause appreciable transport on their own [12,13], and the measured level of transport through the ExB velocity, $\mathbf{v}_E = (c/B^2)\mathbf{E}\times\mathbf{B} \approx (c/B^2)\mathbf{B}\times\nabla_\perp\phi$, is sufficient to account for the level of transport inferred from power balance studies [5].

There is a bit of a paradox here, however. On the theoretical level, collisional drift wave disturbances with $k_\perp \rho_s \sim 1$ [14,15,16] can be taken to be electrostatic if the plasma beta, for drift dynamical studies given by $\beta = 4\pi n T_e/B^2$, satisfies $\beta \ll m_e/M_i$ [17], and in more collisional cases, $\beta \ll (L_\perp/L_\parallel)^2$, where $L_\parallel$ is a typical parallel scale length controlled by the geometry [18]. In more heuristic terms, the electron dynamics is electrostatic if either electron inertia or resistivity are stronger than magnetic induction in the parallel response, and additionally the parallel Alfvén transit frequency must be much faster than any drift wave freqeuency. These conditions are indeed satisfied in the extreme edge regions investigated with probes. This leads to a electrostatic fluid dynamics paradigm, which for the electrons means drift waves and their associated turbulence [19,20]. However, this judgment depends on the scale of motion, since the electron dynamics is excited through the parallel current but the magnetic field responds through the parallel magnetic potential, which are related by $J_\parallel = -(c/4\pi)\nabla_\perp^2 A_\parallel$. Since the observed scale of motion is rather larger than ρ_s, the transition to an electromagnetic response can occur at a β

significantly below m_e/M_i, but how important that turns out to be will clearly depend on the spectrum: not only of the fluctuations themselves but of the source and sink processes (*e. g.*, the rate of fluctuation free energy tapping from the background gradients, or the rate of collisional dissipation). This is important since the dominant energy source region is often at a somewhat smaller scale than the spectrum peak [21,22]. Furthermore, as plasma parameters leave the cold edge regime behind and approach and cross the regime where the L-H transition phenomenon occurs, β is found to be quite close to m_e/M_i and in the H-mode regime it is larger [23]. This means that in those regimes the parallel response will be principally electromagnetic at all important scales of motion.

On the other hand, the question of whether the parallel electron response is electromagnetic is different from the question whether the transport is electrostatic or electromagnetic. The first involves whether magnetic induction, resistivity, or electron inertia controls how fast $J_\parallel$ responds to parallel gradients in the three main state variables ϕ, n, and T_e. This is principally a linear question: how important is $\partial A_\parallel/\partial t$? The second question involves purely nonlinear phenomena: is the ExB transport by $\widetilde{\mathbf{v}}_E$ fluctuations, appearing through the $\mathbf{v}_E \cdot \nabla$ advective derivative, or the magnetic transport by $\widetilde{\mathbf{B}}$ fluctuations, appearing through the perturbed parallel gradient, $\widetilde{\nabla}_\parallel = B^{-1}\widetilde{\mathbf{B}} \cdot \nabla$, also called "magnetic flutter" [24], the more important? One of the results of this work is that "the turbulence is electromagnetic but the transport is electrostatic", *i. e.*, magnetic induction is usually most important to the parallel response but the ExB velocity is more important to the actual transport. Transport by magnetic flutter is usually a small fraction of the ExB transport, even if it becomes significantly different from zero as the edge beta limit (ideal ballooning) is approached.

A separate question is the importance of electron collisions, controlled by the collision frequency, ν_e. The collisional drift wave model depends on resistivity being larger than inertia, even if the response is electromagnetic. Note that this impacts both the current and the parallel heat flux, $q_\parallel$, both of which have constitutive relations to ϕ, n, and T_e in the collisional drift wave limit [15,21]. Even in electromagnetic extensions, most fluid dynamical models leave parallel conductivity as if it were collisional, sometimes flux limiting the conductivity such that $q_\parallel$ is never larger than the "thermal maximum", which is of order nT_eV_e, where $V_e = \sqrt{T_e/m_e}$ is the electron thermal velocity [22,25,26]. As the L-H transition regime is approached the collisionality becomes rather weak at important scales of motion, not only in the sense of a long mean free path, which can be treated by flux limiting, but even compared to $\partial/\partial t$, which cannot. Even in the probe experiments, the only reason that the collisionality isn't judged to be small is that while $\nu_e \lesssim c_s/L_\perp$, the scale of motion is large enough to keep $\omega_* \ll c_s/L_\perp$, and hence $\omega_* \ll \nu_e$. By contrast, the L-H transition regime is characterised by $\beta \sim m_e/M_i$ and $\nu_e \sim \partial/\partial t$, so not only is it marginally electromagnetic, it is also marginally collisional.

It is worth noting that the reason the tokamak edge at the L-H transition is actually in this exotic double marginal regime is that the profile gradients are so steep. Most work on tokamak turbulence assumes that in collisionless regimes the passing (non-trapped) electrons are adiabatic since $V_e/qR \ll \omega$, where ω is the wave frequency of a linear instability, R is the tokamak major radius, and q gives the average pitch of a field line such that the length along B for one turn around the poloidal cross section is $2\pi qR$ [19]. The inequality implies that the transit frequency, V_e/qR, is fast enough to average any electron thermodynamic quantity along the magnetic field before the wave can respond, leading to the bounce averaged models for trapped electrons [27]. But that is not true at edge parameters at the L-H transition with $L_\perp \sim 2\,\mathrm{cm}$ and $qR \sim 500\,\mathrm{cm}$ [23], such that the ratio $(c_s/L_\perp)(qR/V_e)$ is of order 3. This means that there exist drift modes with $k_\perp \rho_s < 1$ for which $V_e/qR \sim \omega_*$. This in turn means that turbulence at diamagnetic frequencies can effectively compete with parallel electron dynamics, allowing the nonlinear instability in drift wave turbulence [28] to robustly function. With regard to collisions, the parameter $\nu_e L_\perp/c_s$ is of order 0.5 and smaller (the significant exception is Alcator C-Mod [29]), which means that there exist drift modes with $k_\perp \rho_s < 1$ for which $\nu_e \sim \omega_*$. This means that electron inertia effects — time delays in the response of $q_\parallel$ as well as $J_\parallel$ — are important, and that Landau damping has to be modelled. Lastly, the ratio $(c_s/L_\perp)(qR/v_A)$, where $v_A = B/\sqrt{4\pi n M_i}$ is the Alfvén velocity, is also of order 3, which means that there will be significant coupling between ExB turbulence and Alfvén waves. In this regime, drift modes are better called "drift Alfvén waves" rather than drift waves [17]. Note that since V_e is not dissimilar to v_A and $k_\perp \rho_s \sim 1$ is within the smaller scale part of the spectrum, the Alfvén waves are kinetic [30], with a significant thermal component.

What is done in this paper is to construct a transcollisional model for electrons [31,32], which can address all of these regimes: electrostatic or electromagnetic, collisional or collisionless. This is important since different parts of the fluctuation spectrum can be in different regimes since the entire dynamics is marginal with respect to both boundaries. The drift approximation with $E_\perp = -\nabla_\perp \phi$ is still used for the perpendicular dynamics, since at these scales ($k_\perp L_\perp \gg 1$) the turbulence is low frequency with respect to compressional Alfvén/lower hybrid waves as well as the gyrofrequencies. The shear Alfvén magnetic fluctuations are retained through $A_\parallel$, with $E_\parallel = -c^{-1}\partial A_\parallel/\partial t - \nabla_\parallel \phi$ and $A_\parallel$ retained in $\nabla_\parallel$. Electron inertia is kept in the equations for both $J_\parallel$ and $q_\parallel$, with a simple dissipation model for Landau damping on $q_\parallel$ which is consistent with the principal effect of previous effort [33] while avoiding the use of the parallel wavenumber $k_\parallel$ in formulae since $\nabla_\parallel$ is nonlinear. The cold ion restriction is still used; incorporation of a finite difference gyrofluid model is the next step after this one (and the gyrofluid effort has yet to incorporate passing electron dynamics [34]). This is the first drift turbulence computation to incorporate both transcollisional and electromagnetic effects, treating T_e and $q_\parallel$ at the same level of sophistication as n and $J_\parallel$, in three dimensions with adequate resolution. The model

builds on the drift Alfvén transport model of Callen [24] and the finite beta universal mode transport model of Molvig *et al* [35], except that the transport is not assumed and not found to be electromagnetic. Some insight into the emergence of electromagnetic effects with rising beta is available from two dimensional studies [36] and early three dimensional ones [37]. The two dimensional studies show that the principal effect of magnetic induction in turbulence is to make the electrons nonadiabatic in the same was as collisions do, by delaying the parallel response to forces and so allowing robust electron driven turbulence. The early three dimensional studies found the magnetic flutter transport to be small in simple geometry. These were limited by available computational resources, however, and therefore were unable to detect the drift Alfvén physics, including the nonlinear instability, to the extent that is possible today.

The principal result of this paper is that the turbulence resulting from this generalised electron fluid dynamics is of the drift Alfvén type. The main mechanism is what can be called the drift Alfvén nonlinear instability — it is the electromagnetic version of the drift wave nonlinear instability [28], and in this electromagnetic regime it is stronger due principally to the fact that magnetic induction emerges with rising beta to slow the electron parallel dynamics through a slower Alfvén velocity. Although there is quantitative sensitivity to magnetic curvature and collisionality, the turbulence and its character does not depend on these additional ingredients: the same qualitative behaviour and the same scaling *vis-a-vis* the plasma beta is observed when curvature and collisional dissipation terms are removed.

Concerning the transport, although the internal dynamics of the turbulence is strongly electromagnetic, both particle and thermal energy transport are dominantly due to turbulent advection the ExB velocity. One can say that the transport is ExB transport, but the level of the ExB velocity disturbances causing that transport is determined by the electromagnetic internal dynamics — the turbulence is electromagnetic but the transport is electrostatic. The point at which the electromagnetic effects become important is roughly $\hat{\beta} = \beta(qR/L_\perp)^2 \gtrsim 1$, roughly similar to the result found by two dimensionsional computations [36], and to the conclusions in linear drift wave analysis [18]. In three dimensions with moderate magnetic shear, however, the turbulence and transport levels sharply increase with β, reflecting the greater strength of the electromagnetic drift Alfvén nonlinear instability. Aside from $\hat{\beta}$, the parameter to which the turbulence was seen to be most sensitive is the magnetic shear, $S = d\log q/d\log x$, where x is the distance in the direction down the profile gradient. At low values of S the sensitivity is minimal since the parallel limitation length is the connection length, $2\pi qR$. At $S \approx 0.5$ the shear limits the parallel length to values below $2\pi qR$ and the turbulence drive levels decrease as S rises further. This leads to more adiabatic electron dynamics and hence to lower gradient drive rates.

It is important to understand that although there is some sensitivity to the magnetic curvature parameter, $\omega_B = 2L_\perp/R$, the turbulence at typical L-H transition parameters

of $\hat{\beta}$ about 10, β about m_e/M_i, and ω_B about 0.03 is in no way of the ballooning mode type. This is made clear by the very weak effect of setting ω_B to zero, especially well into the drift Alfvén regime. Magnetic curvature, like collisional dissipation in this case, should be thought of as an additional perturbation which is applied to an already existing drift Alfvén turbulence and having to compete with it for dominance. The effect of magnetic curvature is simply to cause a small charge buildup on the trailing edge of a pressure disturbance with $\widetilde{p} > 0$, and on the leading edge of a disturbance with $\widetilde{p} < 0$, in the electron drift direction. The effect is to add to the set of effects causing the average phase of $\widetilde{p}$ to be ahead of $\widetilde{\phi}$, for each wave in the overall collection. But the addition is in this case merely a somewhat small enhancement (see also [22]). Magnetic curvature has a strong effect on poloidal asymmetry of the turbulence, but not on the spectrum, energetics, or at $\hat{\beta} \sim 10$ even on the transport level. When the product $\hat{\beta}\omega_B$ (which is synonymous with the MHD ballooning parameter) is further increased, however, sensitivity to ω_B is greater and the ballooning regime is gradually entered, still well below the ideal MHD ballooning threshold. The reason is likely to be the partial cancellation between $\nabla_\parallel p$ and $ne\nabla_\parallel \phi$ in the electron force balance, reducing the strength of the stabilising effect of field line bending, as pointed out by Callen and Hegna [38].

Preliminary versions of both this work [39], and a parallel one by Rogers *et al* [40] neglecting temperature and finite m_e effects, have been presented elsewhere. The second one more decisively found the turbulence strength to increase with β, but the focus was entirely on ballooning — the concepts of drift Alfvén turbulence or electromagnetic nonlinear instability are nowhere mentioned. The first one did note that instability, but the turbulence was found to have a maximum at β close to m_e/M_i. This work did not confirm that, and the maximum may be the result of unrealistic profile evolution in the preliminary treatment. These issues are both clarified here, individually and with respect to each other, for the first time.

Following sections describe the emergence of magnetic induction with rising β, construction of the model equations and their free energy theorem, linear wave properties, the presentation of the results, and the relevance to the parameter domain of the L-H transition in tokamaks. The conclusions are discussed in more detail in their own section.

2. Electromagnetic Fluctuations — the Role of Magnetic Induction

This section is a discussion of how electron inertia replaces the role of collisional dissipation to provide a generalised resistivity for wavelike disturbances, as has been pointed out in collisionless reconnection studies [41], and how Landau damping similarly replaces thermal conduction, when the electron collision damping frequency, ν_e, is no longer large enough to dominate the parallel response to forces. What must be done in a fluid model, then, is to treat both the temperature and parallel heat flux as dynamical variables with the same level of sophistication reserved for the density and parallel current. Hereafter, we restrict to quasineutral plasma and cold ions,such that $n_i = n_e = n$ and $T_i \ll T_e = T$. Since $\nabla_\parallel \ll \nabla_\perp$ at drift scales, only the parallel component of the magnetic potential is treated [42,43], and ψ is written for $A_\parallel$.

In the electrostatic, collisional model of drift waves [14,15,16] and their turbulence [20,21,44], the Ohm's law is a balance between pressure and electric forces on the one hand and resistive friction on the other:

$$m_e \nu_e \frac{1}{e} J_\parallel - \alpha n \nabla_\parallel T = \nabla_\parallel p - ne\nabla_\parallel \phi, \tag{1}$$

where α is the thermal force coefficient (0.71 for pure hydrogen [45]), and the term it multiplies is set on the left side because it is itself part of the frictional dissipation — it exists because the collision frequency depends on particle velocity and hence vanishes if there are no collisions [45,46]. Expressing it in terms of the heat flux is actually more appropriate. The latter is given by

$$q_\parallel + \alpha T \frac{1}{e} J_\parallel = -\kappa n \frac{T}{m_e \nu_e} \nabla_\parallel T \tag{2}$$

(where κ is the thermal conductivity coefficient, equal to 1.6 for pure hydrogen [45]), which suggests that Eq. (1) be rewritten as

$$m_e \nu_e \left[\frac{1}{e} J_\parallel + \frac{\alpha}{\kappa} \left(\frac{1}{T} q_\parallel + \alpha \frac{1}{e} J_\parallel \right) \right] = \nabla_\parallel p - ne\nabla_\parallel \phi, \tag{3}$$

and Eq. (2) as

$$\frac{1}{\kappa} m_e \nu_e \left(\frac{1}{T} q_\parallel + \alpha \frac{1}{e} J_\parallel \right) = -n \nabla_\parallel T. \tag{4}$$

This representation of the two equations has the advantage of showing the essential symmetry between the parallel current and heat flux, both expressed as fluxes in response to forces, and the mixing between them represented by a nonzero α shows, in a less mysterious way than usual, the symmetry (Onsager symmetry) inherent in the thermal force (see also [47].

This preliminary discussion sets the stage for the introduction of both electromagnetic (finite β) and inertial (finite m_e, or collisionless) effects. What will become apparent is simply that the frictional component in both these balances (Eqs. 3,4) is replaced by either or both electromagnetic and inertial effects. A finite β brings in the magnetic fluctuations in two ways. First, magnetic induction adds to the parallel electric field,

$$E_{\|} = -\frac{1}{c}\frac{\partial \psi}{\partial t} - \nabla_{\|}\phi, \tag{5}$$

where ψ is the parallel component of the magnetic potential, and the perturbed magnetic field is

$$\widetilde{\mathbf{B}} = \nabla \times \psi \mathbf{b} \approx -\mathbf{b} \times \nabla \psi. \tag{6}$$

Second, the parallel gradient picks up a nonlinear component due to the perturbation of $\mathbf{B}$, called "magnetic flutter," [24]

$$\widetilde{\nabla}_{\|} = \frac{1}{B}\widetilde{\mathbf{B}} \cdot \nabla \approx -\frac{1}{B^2}\mathbf{B} \times \nabla \psi \cdot \nabla. \tag{7}$$

Magnetic induction is separately important because it affects the linear response of the current to forces, and hence the speed of waves and their dissipation. As is well known, it replaces the resistive friction as the controller of the response,

$$\frac{ne}{c}\frac{\partial \psi}{\partial t} + m_e \nu_e \left[\frac{1}{e}J_{\|} + \frac{\alpha}{\kappa}\left(\frac{1}{T}q_{\|} + \alpha\frac{1}{e}J_{\|}\right)\right] = \nabla_{\|}p - ne\nabla_{\|}\phi, \tag{8}$$

in the left side of which the induction term dominates if β is high enough. Specifically, since $J_{\|}$ and ψ are related through the Ampere's law, $(4\pi/c)J_{\|} = -\nabla^2\psi$, induction overshadows resistive friction if the perpendicular scale is larger than the collisional skin depth, or if $\beta > (\nu_e/\omega)(k_{\perp}\rho_s)^2(m_e/M_i)$[48, 49], where $\beta \equiv 4\pi nT/B^2$ and ω is a typical frequency of the dynamics.

Magnetic induction does not, however, affect the heat flux, except indirectly through its effect on the current. Whether the collisional friction term is dominant or not in controlling the response of $q_{\|}$ to the thermal gradient is independent of β. What this does depend on is the electron mass — if the collision frequency is low enough compared to dynamical time scales then the inertia will replace friction. Unfortunately, the fluid equations lose their validity at the same point. It is possible to construct a model in which the important physical phenomena are captured while still preserving a low order moment, or fluidlike, approach [33,34]. In this work, such a model is constructed by a simple fluid closure scheme in which the fourth velocity moment is that given by a perturbed Maxwellian distribution function up to a correction which models Landau damping. The Landau damping term is chosen to take into account the fact that $k_{\|}$ cannot be used as a parameter when $\nabla_{\|}$ is a nonlinear operator. The simplest way to do this is a direct

damping coefficient for $q_\parallel$ which gives the correct damping rate for the longest parallel wavelengths (we are implicitly assuming that the longest wavelengths are dominant in $q_\parallel$). A factor of 5/2 arises in front of the $\nabla_\parallel T$ term in the construction of the fourth moment; taking this into account with the collisional limit in Eq. (4), we have

$$\frac{m_e}{T}\left(\frac{\partial}{\partial t}+\mathbf{v}_E\cdot\nabla\right)q_\parallel=-\frac{5}{2}n\nabla_\parallel T-\frac{m_e}{T}a_L q_\parallel-\frac{5/2}{\kappa}m_e\nu_e\left(\frac{1}{T}q_\parallel+\alpha\frac{1}{e}J_\parallel\right), \qquad (9)$$

where $a_L = V_e/qR$, $L_\parallel = 2\pi qR$ is the parallel system size, and $V_e = (T/m_e)^{1/2}$ is the electron thermal velocity. The frictional dissipation term has been moved to the right side. Note that a_L as a time independent damping is equivalent to what is often called a Knudsen correction [25]. In a local model under drift ordering, nonlinear effects in this equation are limited to $\partial/\partial t$ becoming an ExB advective derivative and the contribution of magnetic fluctuations to $\nabla_\parallel$ [21,49]. In a completely nonlinear model conservation considerations cause several parallel advection terms like $m_e e^{-1}J_\parallel\nabla_\parallel$ and $u_\parallel\nabla_\parallel$ to arise, but under drift ordering they are small [21,50].

In the Ohm's law the inertia appears normally,

$$\frac{ne}{c}\frac{\partial\psi}{\partial t}+m_e\frac{1}{e}\left(\frac{\partial}{\partial t}+\mathbf{v}_E\cdot\nabla\right)J_\parallel=\nabla_\parallel p-ne\nabla_\parallel\phi-m_e\nu_e\left[\frac{1}{e}J_\parallel+\frac{\alpha}{\kappa}\left(\frac{1}{T}q_\parallel+\alpha\frac{1}{e}J_\parallel\right)\right], \qquad (10)$$

and introduces the collisionless skin depth as the perpendicular scale above which the induction becomes dominant in the weakly collisional and collisionless regimes: this happens if $\beta > (k_\perp\rho_s)^2(m_e/M_i)$ [17]. It is important to note the absence of ExB advection acting directly upon ψ. This leads to the absence of ExB transport of current or the magnetic field at large scale where the electron inertia is negligible, and is the reason why there is no appreciable anomalous resistivity in magnetically confined plasmas in equilibrium [51]. Since a non-collisional resistivity is likewise to be avoided, the Landau damping term is applied only to $q_\parallel$ and not also to $J_\parallel$. Energetic considerations also suggest against a direct or viscous like damping on $J_\parallel$ [33].

Introducing the collisionless and electromagnetic effects in the above order makes clear the essential relationship between drift waves and drift Alfvén waves [17]. Drift waves result if the response is parallel electron response to forces is electrostatic. The limit of validity for this in turbulence is much more severe than has been appreciated. The limit is often stated as $\beta < m_e/M_i$ [17], but we can see that this depends on the implicit assumption that $k_\perp\rho_s \sim 1$ for drift waves (see also [18] on this). Years of study of drift wave turbulence have shown the importance of much longer wavelengths (*e. g.*, [20,21,22]). Experimental observations of tokamak edge turbulence also show that the dominant scales are much larger than ρ_s [5–12]. It follows that the dynamics is electromagnetic in character even down towards the very low values of β found in typical $T_e < 50\,\mathrm{eV}$ scrape off layers in which

the majority of the probe experiments have been done: a typical $k_\perp \rho_s \sim 0.03$ leads to the conclusion that the dominant scales are electromagnetic even for $\beta \sim 10^{-6}$. This does not mean that the transport should be electromagnetic or even that what has been learned from study of drift waves need be discarded. All that matters is that magnetic induction enters to control the response of nonadiabatic transients to parallel forces: a disturbance cannot propagate along the magnetic field, whether wavelike or diffusively, faster than the Alfvén velocity, $v_A = B(4\pi n M_i)^{-1/2}$, or at arbitrarily small scale faster than V_e. This is principally a quantitative effect to each scale of motion, since the turbulence is still well described as an interaction between nearly two dimensional ExB turbulence perpendicular to the magnetic field and parallel, nonadiabatic electron transients parallel to the magnetic field. The dynamics is still electrostatic in the perpendicular plane, since $k_\perp v_A$ and the lower hybrid frequency are both very large compared to ω, and hence the perpendicular velocities and fluxes are described by their drifts, both ExB and diamagnetic.

It is of the greatest importance to keep in mind that although some of the above results may remind one of the transition to ideal MHD with increasing scale, at no time will it become valid for gradient driven microturbulence that the pressure should drop out of the Ohm's law. To state it specifically, the simple resistive MHD Ohm's law, $\mathbf{E}+c^{-1}\mathbf{v}\times\mathbf{B} = \eta\mathbf{J}$, is never valid if the typical frequencies are not greater than diamagnetic, even for arbitrarily large spatial scale. Only when the ideal ballooning limit is crossed will the dynamical time scale be so short. By contrast, gradient driven drift turbulence models must always additionally keep the pressure, such that one has at minimum $\mathbf{E} + \nabla p_e + c^{-1}\mathbf{v}\times\mathbf{B} = \eta\mathbf{J}$. This is the principal shortcoming of resistive g [52] and current diffusion [53] models.

3. Electromagnetic Drift Wave Equations and Energetics — Isotropic Temperature

For now the temperature is assumed to be isotropic: there are three degrees of freedom, and there is only one each of temperature and parallel heat flux. Drift ordering is assumed, according to which ExB advection and the perturbed $\nabla_\parallel$ are the only nonlinearities.

Normalisation is in terms of drift scales: $\nabla_\perp$ appears as $\rho_s\nabla_\perp$, $\nabla_\parallel$ as $qR\nabla_\parallel$, and $\partial/\partial t$ as $(L_\perp/c_s)(\partial/\partial t)$. The eight dependent variables are normalised as ϕ to T_e/e, n and T to n_e and T_e, $u_\parallel$ to $c_s qR/L_\perp$, $J_\parallel$ to $n_e e c_s qR/L_\perp$, $q_\parallel$ to $n_e T_e c_s qR/L_\perp$, ψ to $B\rho_s\beta qR/L_\perp$, and Ω to $\rho_s^{-2}T_e/e$. The dependent variables are further scaled by a factor of the drift parameter, $\delta = \rho_s/L_\perp$, *e. g.*, $\phi \leftarrow \delta^{-1}e\phi/T_e$. In these expressions $L_\perp$ is the profile scale, $c_s = (T_e/M_i)^{1/2}$, and $\rho_s c_s = cT_e/eB$.

The full system of equations is given by

$$\left(\frac{\partial}{\partial t} + \mathbf{v}_E\cdot\nabla\right)\Omega = \nabla_\parallel J_\parallel - \mathcal{K}(T+n), \tag{11}$$

$$\hat{\beta}\frac{\partial}{\partial t}\psi + \hat{\mu}\left(\frac{\partial}{\partial t} + \mathbf{v}_E\cdot\nabla\right)J_\parallel = \nabla_\parallel(T+n-\phi) - \hat{\mu}\nu\left[J_\parallel + \frac{\alpha}{\kappa}\left(q_\parallel + \alpha J_\parallel\right)\right], \tag{12}$$

$$\left(\frac{\partial}{\partial t} + \mathbf{v}_E\cdot\nabla\right)n = -\omega_n\frac{\partial\phi}{\partial y} + \nabla_\parallel(J_\parallel - u_\parallel) - \mathcal{K}(T+n-\phi), \tag{13}$$

$$\frac{3}{2}\left(\frac{\partial}{\partial t} + \mathbf{v}_E\cdot\nabla\right)T = -\frac{3}{2}\omega_t\frac{\partial\phi}{\partial y} + \nabla_\parallel(J_\parallel - u_\parallel - q_\parallel) - \mathcal{K}(3.5T+n-\phi), \tag{14}$$

$$\hat{\mu}\left(\frac{\partial}{\partial t} + \mathbf{v}_E\cdot\nabla\right)q_\parallel = -\frac{5}{2}\nabla_\parallel T_e - \hat{\mu}a_L q_\parallel - \hat{\mu}\nu\frac{5/2}{\kappa}\left(q_\parallel + \alpha J_\parallel\right), \tag{15}$$

$$\hat{\epsilon}_s\left(\frac{\partial}{\partial t} + \mathbf{v}_E\cdot\nabla\right)u_\parallel = -\nabla_\parallel(n+T) - \mu_\parallel\nabla_\parallel^2 u_\parallel, \tag{16}$$

and the two auxiliary relations for the vorticity and current,

$$\Omega = \nabla_\perp^2\phi, \qquad J_\parallel = -\nabla_\perp^2\psi, \tag{17}$$

with $\mathbf{v}_E\cdot\nabla$ representing advection by the ExB velocity and the nonlinear parallel gradient $\nabla_\parallel$ including the contributions from ψ.

The geometry is a three dimensional sheared flux tube model, with the simple ballooning approximation for the toroidal magnetic curvature effects [54,55]. Leaving the more proper tokamak geometry [22,56,57] to subsequent papers as mentioned below allows a better understanding of the differences between intrinsic physics and that dependent on the details of the geometry (see [22], where these were combined in the context of a nonlocal model). Given the cylindrical coordinates (r,θ,ζ), the slab like coordinates (x,y,s) are defined to follow the unperturbed field lines:

$$x = r - a, \qquad y = \frac{a}{q_a}(q\theta - \zeta), \qquad s = q_a R\theta,$$

where a is the reference minor radius, R is the major radius, and q_a is a normalising constant allowing y and s to be defined as simple distances. The factor of q in y is variable, allowing for shear through the parameter $S = d\log q/d\log x$. In normalised units, the computational domain and boundary conditions are x bounded on $[-x_L, x_L]$, y periodic on $[0, 2\pi/K]$, and s quasiperiodic on $[-\pi, \pi]$. Dependent variables vanish for $x = \pm x_L$, and quasiperoidicity in s means the variables take identical values at $(y + 2\pi Sx, s + 2\pi)$ and (y, s). This is the parallel boundary condition, also called the periodicity constraint (dependent variables are periodic in both θ and ζ), whose importance is discussed elsewhere [22]. In all cases, the grid was $64 \times 256 \times 16$ nodes in (x, y, s), with $x_L = 32$ and $K = 0.025$. This makes the domain in the perpendicular plane $64 \times 256\rho_s$, corresponding to about $2.5 \times 10\,\mathrm{cm}$ for typical tokamak edge parameters at the L-H transition [1,23].

In this model the differential operators are

$$\nabla_\perp^2 = \left(\frac{\partial}{\partial x} + Ss\frac{\partial}{\partial y}\right)^2 + \left(\frac{\partial}{\partial y}\right)^2, \tag{18}$$

for the perpendicular Laplacian, and

$$\mathbf{v}_E \cdot \nabla = \nabla s \times \nabla\phi \cdot \nabla, \qquad \nabla_\parallel = \frac{\partial}{\partial s} - \hat{\beta}\nabla s \times \nabla\psi \cdot \nabla,$$

for ExB advection and the parallel gradient. Magnetic curvature is modelled with

$$\mathcal{K} = \omega_B \left(\cos s \frac{\partial}{\partial y} + \sin s \frac{\partial}{\partial x}\right),$$

which is the lowest order contraction of $\nabla \log B^2$ with $\nabla s \times \nabla$.

In addition to α and κ, the main parameters controlling the kinetic Alfvén wave speeds,

$$\hat{\beta} = \frac{4\pi n T_e}{B^2}\left(\frac{qR}{L_\perp}\right)^2 = \left(\frac{c_s/L_\perp}{v_A/qR}\right)^2, \qquad \hat{\mu} = \frac{m_e}{M_i}\left(\frac{qR}{L_\perp}\right)^2 = \left(\frac{c_s/L_\perp}{V_e/qR}\right)^2,$$

secondary parameters,

$$\nu = \frac{\nu_e}{c_s/L_\perp}, \qquad \omega_B = 2\frac{L_\perp}{R}, \qquad \omega_n = \frac{L_\perp}{L_n}, \qquad \omega_t = \frac{L_\perp}{L_T},$$

and auxiliaries $\hat{\epsilon}_s$, a_L, and S (magnetic shear), are all constants. The nominal value of $\hat{\epsilon}_s$ is $(qR/L_\perp)^2$, but it can be set smaller than this in order to speed up the parallel ion dynamics. The Landau damping parameter is usually set to $a_L = (V_e L_\perp / c_s qR)$.

The fluctuation free energy theorem for this model is constructed in the same way as for the collisional drift wave model [21]. The energy is defined as

$$E = \frac{1}{2}\int d^3V \left[|\nabla_\perp \phi|^2 + n^2 + \frac{3}{2}T^2 + \left(\hat{\beta}\psi + \hat{\mu}J_\parallel\right)J_\parallel + \frac{2}{5}\hat{\mu}q_\parallel^2 + \hat{\epsilon}_s u_\parallel^2\right], \tag{19}$$

with the domain integral $\int d^3V$ normalised such that $\int d^3V(1) = 1$. The energy evolves following Eqs. (11–17) according to

$$\frac{1}{2E}\frac{\partial E}{\partial t} = \Gamma_n + \Gamma_t + \Gamma_{jm} + \Gamma_{qm} - \Gamma_c - \Gamma_k - \Gamma_l - \Gamma_s. \tag{20}$$

The first four contributions in Eq. (20) are the sources, also called drive terms. These are split into the two groups of gradient drive due to ExB advection, Γ_n and Γ_t, and gradient drive due to magnetic flutter, Γ_{jm} and Γ_{qm}, which are given by

$$\begin{aligned} \Gamma_n &= -\frac{1}{2E}\int d^3V\, \omega_n n \frac{\partial \phi}{\partial y}, & \Gamma_{jm} &= \frac{1}{2E}\int d^3V\, \hat{\beta}(\omega_n + \omega_t)\left(u_\parallel - J_\parallel\right)\frac{\partial \psi}{\partial y}, \\ \Gamma_t &= -\frac{1}{2E}\int d^3V\, \frac{3}{2}\omega_t T \frac{\partial \phi}{\partial y}, & \Gamma_{qm} &= \frac{1}{2E}\int d^3V\, \hat{\beta}\omega_t q_\parallel \frac{\partial \psi}{\partial y}, \end{aligned} \tag{21}$$

in which $-\partial\phi/\partial y$ is the down gradient component of $\mathbf{v}_E$ and $\partial\psi/\partial y$ is the down gradient component of $\widetilde{\mathbf{B}}$.

The next four contributions in Eq. (20) are the sinks. These are the two collisional dissipation sinks — resistivity, Γ_c, and thermal conductivity, Γ_k — and Landau damping, Γ_l, and ion sound dissipation, Γ_s, all given by

$$\begin{aligned} \Gamma_c &= \frac{1}{2E}\int d^3V\, \hat{\mu}\nu J_\parallel^2, & \Gamma_l &= \frac{1}{2E}\int d^3V\, \frac{2}{5}\hat{\mu}a_L q_\parallel^2, \\ \Gamma_k &= \frac{1}{2E}\int d^3V\, \frac{\hat{\mu}\nu}{\kappa}\left(q_\parallel + \alpha J_\parallel\right)^2, & \Gamma_s &= \frac{1}{2E}\int d^3V\, \mu_\parallel \left|\nabla_\parallel u_\parallel\right|^2, \end{aligned} \tag{22}$$

In the deeply collisional regime ($\nu\hat{\mu} \gg {k_\parallel}^2$), Γ_l is small, and Γ_c and Γ_k revert to their collisional forms, given in [21]. It is important to note that no effects associated with compressibility enter Eqs (20–22). Parallel compressions go through $\nabla_\parallel$ and perpendicular ones go through the curvature, $\mathcal{K}$. Curvature is a transfer phenomenon just like the compressional effects in sound waves, *i. e.*, it should not be thought of as potential energy, as in many older treatments. It destabilises disturbances in both drift wave and drift Alfvén limits, through compression of the diamagnetic current which tends to cause a wave in ϕ to lag behind one in $(n + T)$ in the y direction if the local curvature vector is aligned with the pressure gradient. As in the electrostatic regime [22], this results in a positive (or more positive) phase shift of n ahead of ϕ, hence strengthening the combined gradient ExB drive $(\Gamma_n + \Gamma_t)$.

Sources of fluctuation free energy are limited to the background density and temperature gradients, acting through both ExB advection and magnetic flutter. These are related to ExB and magnetic flutter transport in the obvious way. If ω_n and ω_t are set to zero, E must decrease monotonically, and cannot be driven by such subsidiary effects as curvature.

Several effects present in the generally nonlinear case are not carried in these equations: finite T_i, full flux surface geometry, parallel advection (terms like $m_e e^{-1} J_\parallel \nabla_\parallel$ and $u_\parallel \nabla_\parallel$), and Pfirsch-Schlüter effects (further variation of ω_B with s leading to a nonzero flux surface average of $\mathcal{K}$). It is important to establish the intrinsic dynamics before moving on, so that the physics of drift Alfvén turbulence is not confused with other effects. Sorting out the various roles of magnetic induction and flutter, and ballooning, is enough for the moment.

4. Linear Properties

The linear properties of the model described by Eqs. (11–17) are best understood by first considering their parallel and perpendicular effects separately, and then looking at the combination which results from their interaction. The following discussion is intended only to provide insight into the linear properties in general; there is no need to introduce complicated geometry or tokamak effects, or even magnetic shear.

If both ν and a_L are neglected, the parallel dynamics is purely hyperbolic, so that the linear properties can be studied through the resulting wave speeds. Neglecting the background gradients, the ion motion, and the temperature, all limits of the Alfvén wave become clear in the following dispersion relation:

$$\omega^2 = {k_\parallel}^2 \frac{1 + k_\perp^2}{\hat{\beta} + \hat{\mu} k_\perp^2}, \tag{23}$$

assuming a mode dependence of $\exp[i(\mathbf{k}_\perp \cdot \mathbf{x}_\perp k_\parallel s - \omega t)]$. This is the cold ion limit of the kinetic Alfvén wave [30]. At large perpendicular scale (low $k_\perp$), the ideal MHD Alfvén wave is recovered. As $k_\perp$ increases, the parallel electron response causes departure from the ideal $E_\parallel = 0$. This reflects the importance of the perturbed pressure in the Ohm's law, Eq. (12), and hence one of the validity limits of one fluid MHD: that $k_\perp$ should be small. When the perpendicular scale becomes smaller than the collisionless skin depth, or equivalently when $\hat{\beta} < \hat{\mu} k_\perp^2$, the electron response becomes electrostatic and the wave speed is the electron thermal speed, V_e, rather than the Alfvén speed, v_A. This is specifically the finite mass effect, distinct from the dependence of the kinetic Alfvén wave speed on $k_\perp$. (Note here and below that the normalisation factor of $[qR/L_\perp]^2$ is common to $\hat{\beta}$, $\hat{\mu}$, and $\hat{\epsilon}_s$.)

If $u_\parallel$ is not neglected, we recover the four waves associated with ψ, ϕ, n, and $u_\parallel$: two kinetic Alfvén waves and two sound waves, coupled through the dispersion relation,

$$\hat{\epsilon}_s \omega^2 \left[\left(\hat{\beta} + \hat{\mu} k_\perp^2 \right) \omega^2 - \left(1 + k_\perp^2 \right) {k_\parallel}^2 \right] - {k_\parallel}^2 \left[\left(\hat{\beta} + \hat{\mu} k_\perp^2 \right) \omega^2 - {k_\parallel}^2 \right] = 0, \tag{24}$$

well separated if both $\hat{\beta}$ and $\hat{\mu}$ are smaller than $\hat{\epsilon}_s$, or equivalently, if both β and m_e/M_i are small.

If we neglect $u_\parallel$ again but keep T and $q_\parallel$, we find the thermal modifications to the kinetic Alfvén wave:

$$\hat{\mu} \omega^2 \left[\left(\hat{\beta} + \hat{\mu} k_\perp^2 \right) \omega^2 - \left(1 + \frac{5}{3} k_\perp^2 \right) {k_\parallel}^2 \right] - \frac{5}{3} {k_\parallel}^2 \left[\left(\hat{\beta} + \hat{\mu} k_\perp^2 \right) \omega^2 - \left(1 + k_\perp^2 \right) {k_\parallel}^2 \right] = 0, \tag{25}$$

which for $\hat{\beta} \gg \hat{\mu} k_\perp^2$ splits into two kinetic Alfvén waves given approximately by Eq. (30) and two heat waves given by

$$\hat{\mu} \omega^2 = \frac{5}{3} {k_\parallel}^2, \tag{26}$$

propagating at a speed close to V_e. The opposite extreme is short wavelength and low beta, $\hat{\beta} \ll \hat{\mu}$ and $k_\perp^2 \gg 1$, at which the two types of waves merge:

$$\left(\hat{\mu}\omega^2\right)^2 + \frac{10}{3}\hat{\mu}\omega^2 {k_\parallel}^2 + \frac{5}{3}{k_\parallel}^4 = 0, \tag{27}$$

describing kinetic waves propagating at a speed close to V_e. Adding $u_\parallel$ back to this gives the sound waves in addition, again well separated from the Alfvén waves and heat waves if both β and m_e/M_i are small.

Now we turn to the modes that are present when there is a background gradient. For clarity we neglect $u_\parallel$ and the $T, q_\parallel$ pair, but now retain the density gradient, ω_n, and the resistivity, $\hat{\mu}\nu$. This recovers the drift Alfvén wave, which is the electromagnetic analog of the drift wave [17]:

$$\omega^2\left[\hat{\beta}(\omega-\omega_*)+\hat{\mu}k_\perp^2(\omega+i\nu)\right] - \left(1+k_\perp^2\right){k_\parallel}^2\left(\omega - \frac{\omega_*}{1+k_\perp^2}\right) = 0, \tag{28}$$

where $\omega_* = \omega_n k_y$, and in which the resistively damped kinetic Alfvén wave and the drift wave are well separated if the kinetic Alfvén speed implied by Eq. (23) is sufficiently large. Eq. (28) describes three modes: the drift Alfvén wave itself, and the two shear Alfvén transients to which it is coupled [58] (see also [36]).

This is worth examining further: in the limit that both $\hat{\beta}$ and $\hat{\mu}$ are small, meaning that the kinetic Alfvén transit time is short compared to drift wave time scales, the low frequency solution of Eq. (28) is

$$\omega = \omega_L + \frac{\omega_L^2}{\left(1+k_\perp^2\right){k_\parallel}^2}\left[\hat{\beta}(\omega_L-\omega_*)+\hat{\mu}k_\perp^2(\omega_L+i\nu)\right],$$

with the mode frequency given by

$$\omega_L = \frac{\omega_*}{1+k_\perp^2},$$

and the slight growth rate proportional to ν. Because the electron inertia, $\hat{\mu}k_\perp^2\omega_L$, and the magnetic induction, $\hat{\beta}(\omega_L-\omega_*)$, lead only to a slight shift in the frequency away from ω_L, the growth rate is as given in the collisional, electrostatic case [14]. This suggests the usual linear theory interpretation that electromagnetic effects enter the dynamics when $\hat{\beta} \sim 1$ [18]. If $\hat{\mu}\nu k_\perp^2 > \beta\omega$ and $\nu > \omega$, the transients are also electrostatic and collisional. However, the resulting damping rate of transients is very fast:

$$\gamma_d \sim ({k_\parallel}^2/\hat{\mu}\nu)(1+k_\perp^2)/k_\perp^2, \tag{29}$$

which for small $\hat{\mu}$ violates the assumption that $\nu > \omega$.

This is a good way to understand how the standard approach to linear waves breaks down for turbulence: although the linear wave can be in the electrostatic regime for tokamak far edge parameters, the transients never are. For linear waves the eigenmodes evolve separately, but in turbulence they are well coupled, so the electrostatic, collisional model restriction is undesirable. What this means is that even though the linear drift mode may be judged electrostatic, the dissipation of the turbulence going as it does through the transients will be partially wavelike, going through resistively damped kinetic Alfvén waves, which are electromagnetic if $\hat{\beta} > \hat{\mu} k_\perp^2$ The electron response to parallel forces depends on inertia, $\hat{\mu} k_\perp^2 \omega$, induction, $\hat{\beta}\omega$, or resistivity, $\hat{\mu}\nu k_\perp^2$, whichever is *slower*. A generated disturbance will propagate down the field lines a substantial distance before it is dissipated. Moreover, in turbulence the magnetic field lines are displaced by the same wave dynamics, leading to magnetic flutter, which in turbulence reduces coupling and cross coherence among the state variables by comparison to the electrostatic model, as we shall see.

Electromagnetic effects enter the principal branch as well if the kinetic Alfvén transit frequency is no longer arbitrarily fast: if $\hat{\beta} + \hat{\mu} k_\perp^2$ is no longer small, leading to the possibility of a mode crossing. The subtlety of the additional linear gradient term in $\widetilde{\nabla}_\parallel n$ prevents a mode crossing in the pure Alfvén wave, but if $\hat{\mu} > 1$ there is in fact an electrostatic mode crossing. The ideal fluid equations ($\nu = 0$) have an instability there, which in the collisionless regime forces one to face Landau damping in order to have a reasonable model. This specifically requires the retention of both T and $q_\parallel$ as full fledged dynamical variables, as the $T \leftrightarrow q_\parallel$ pair is the only route to Landau damping. Isothermal models are limited to the strictly collisional regime because of the ideal fluid mode crossing. The effect of the Landau damping term, a_L, on the drift wave branch of the full linear dynamics is to allow a consistent dissipation even when ν vanishes, recovering the collisionless universal mode.

To summarise the above, fluid electron drift turbulence is always partially electromagnetic at tokamak edge parameters because the transients are electromagnetic. It is strongly electromagnetic if in addition $\hat{\beta} > 1$ or $\beta \gtrsim m_e/M_i$. This is precisely the regime the tokamak edge at the L-H transition is in.

4a. Ballooning Modes

Here we briefly discuss the effects of magnetic curvature, enough to clarify its mechanism and to understand instabilities of the ballooning type which do not depend on collisions but are nevertheless found below the ideal MHD threshold in β. This is made possible because of the perturbed pressure in the Ohm's law, Eq. (12). As noted in recent work by Callen and Hegna [38], a partial cancellation between $(n+T)$ and ϕ reduces the contribution of the field line bending term, $\nabla_\parallel J_\parallel$, to the mode's stability, allowing the instability to exist below the ideal threshold.

Magnetic curvature acts essentially as a catalyst, as seen by the fact that the $\mathcal{K}$ terms in Eqs. (11–17) act to transfer fluctuation free energy between the dependent variables but do not appear in the sources and sinks, in Eqs. (21,22) [22]. The easiest case to understand is the isothermal, electrostatic resistive ballooning mode, in which $\hat{\mu}\nu J_\parallel = ik_\parallel(n-\phi)$ and $\omega k_\perp^2 \phi = k_\parallel J_\parallel - \omega_C n$, where ω_C is $-i\mathcal{K}$ in Fourier space (note $\mathcal{K}$ is real and positive if the curvature is maximally unfavorable). These two relations determine the response of ϕ to whatever n is, enforcing a given phase relationship for the resulting linear wave:

$$n = \frac{{k_\parallel}^2 - i\hat{\mu}\nu\omega k_\perp^2}{{k_\parallel}^2 + i\hat{\mu}\nu\omega_C}\phi. \tag{30}$$

The factor multiplied by ν in the numerator is what produces the basic collisional drift wave instability in a uniform magnetic field [14], by leading to a lag of ϕ behind n, so that Γ_n in Eqs. (21,22) is positive and the disturbance is driven by the background density gradient. If the curvature is unfavorable, then the factor multiplied by ω_C in the denominator also tends to produce a destabilising phase shift, and it will be stronger in doing so if $\omega_C > \omega k_\perp^2$. Because ω_C is positive on the outside of the torus in a tokamak, and is maximum at the outboard midplane, this curvature induced instability is called a ballooning mode. As long as $\hat{\mu}\nu\omega_C < {k_\parallel}^2$, however (as is always true on closed field lines in a tokamak, especially at long perpendicular wavelength), the basic nature of the disturbance is that of a drift wave whose phase shift happens to be controlled by the magnetic curvature.

Electromagnetic induction enters this mode in the same way as it does for a drift wave. The ideal MHD limit is found by replacing $\hat{\mu}\nu J_\parallel$ with $-i\omega\hat{\beta}\psi$, and neglecting the perturbed pressure in Eq. (12), and everything except the ω_n term in Eq. (13). Aside from the $\omega = 0$ root associated with the neglected $u_\parallel$, we obtain

$$\omega^2 = \frac{{k_\parallel}^2}{\hat{\beta}} - \frac{\omega_*\omega_C}{k_\perp^2},$$

which leads to the ideal threshold. In a tokamak, $k_\parallel \sim 1$ in these units, somewhat modified by finite shear, or S, and $\omega_C\omega_*/k_\perp^2$ is about $\omega_n\omega_B = 2L_n/R$, somewhat modified by flux

surface geometry (the curvature is not everywhere maximally unfavorable). Replacing ∇n with ∇p, or ω_n with $(\omega_n + \omega_t)$, the ideal threshold is $\hat{\beta}(\omega_n + \omega_t)\omega_C \gtrsim 1$, or $\beta q^2 R \gtrsim L_p$ up to constants of order unity which depend on the magnetic geometry [59].

Note, however, that taking the ideal MHD limit breaks the conservation of fluctuation free energy by curvature, which now appears in Eq. (20) as an energy source, as in older treatments. Reinstating the drift effects — all terms in Eq. (13) except $\nabla_\parallel u_\parallel$, and all terms in Eqs. (11,12) except those involving T or ν — this inconsistency is remedied and we arrive at a much more interesting dispersion relation:

$$\omega^2 = {k_\parallel}^2 \frac{\omega\left(1+k_\perp^2\right) - (\omega_* - \omega_C)}{(\omega - \omega_*)\,\hat{\beta} + \omega\hat{\mu}k_\perp^2} - \frac{\omega_*\omega_C}{k_\perp^2} - \left(\omega + \frac{\omega_C}{k_\perp^2}\right)\omega_C, \tag{31}$$

which still in the absence of dissipation can be called "pseudo ideal MHD" — aside from being a properly consistent formulation, it yields a nondissipative ballooning mode below the ideal threshold [38]. This is due to the emergence of the perturbed pressure in the Ohm's law, through the parallel dynamics alone with finite $k_\perp^2$, and through the gradient forcing at the diamagnetic frequency, also essentially at finite $k_\perp$.

It is important to note that the ballooning and drift Alfvén branches are separate. The ballooning modes which are destabilised at the ideal threshold are actually the Alfvén transients discussed above, not the drift Alfvén or drift wave mode. This shows the fundamental difference in their character: the ballooning mode/Alfvén wave branch has to do with a restoring force due to field line bending, and the sign change provoked in that force due to unfavourable curvature. The drift wave/drift Alfvén mode branch is the zero frequency mode which results from taking the ideal MHD limit in Eq. (31); it is actually at $\omega = \omega_*$ as $k_\perp \to 0$. So in the case of drift Alfvén and ballooning modes, we are discussing fundamentally different dynamics.

Moreover, at the threshold we are necessarily discussing low frequencies and $\hat{\beta} > 1$, and this means that for finite $\hat{\mu}$ we run into the ideal mode crossing instability for $\hat{\mu} > 1$. In turn, this forces us to restore the $T \leftrightarrow q_\parallel$ pair and Landau damping. A gradual merger takes place between the basic drift Alfvén instability and the pseudo ideal MHD instability as $\hat{\beta}$ increases, and when $\hat{\mu} > 1$, that merger takes place before even pseudo ideal ballooning is reached, relegating ballooning to secondary importance until the ideal threshold is approached. We will see this in the computational results regarding the turbulence. We will not develop this analysis any further, since the results of the turbulence computations presented in following Sections show very clearly that ballooning has no role in determining the qualitative dynamical character, even when it is quantitatively very important.

To summarise, the model described by Eqs. (11–17) admits a number of important modes, among them Alfvén waves and ideal MHD ballooning modes, drift waves, drift

Alfvén waves, and collisionless universal modes. Which type of linear mode prevails depends on geometry as well as parameters; the foregoing is intended only as a basic survey to show how these different modes are related. As is known, however, what type of transport results from the complete system of equations can only be determined by nonlinear numerical simulation, as the properties of the model in turbulence are very often quite different from what the linear waves would suggest.

5. Results — Basic Character of the Turbulence

This section presents the basic result of this computation series: sensitivity to magnetic fluctuations sets in at $\hat{\beta} \sim 1$, and at larger values the turbulence becomes markedly stronger. The mode structure is qualitatively not different from that found in electrostatic drift wave studies; it is determined by spectral transfer to both longer and shorter wavelengths out of a region of net drive by the gradients. Fluctuation statistics show Gaussian amplitude distributions and low cross coherence, but decidedly nonrandom relative phase distributions showing strong coupling among the state variables (ϕ, n, and T). As $\hat{\beta}$ increases, the degree to which this coupling is maintained weakens. In the Section after this one it is shown that most of this is simply due to the slowing of the Alfvén velocity in relative terms with $\hat{\beta}$, all consistent with the identification of the dynamics as drift Alfvén turbulence.

The nominal case against which all others were compared was the one characterised by $\hat{\beta} = \hat{\mu} = 10$, $\nu = 0.5$, $\omega_B = 0.03$, and $\omega_n = \omega_t = 1$. The computational domain was $64 \times 256\rho_s$ in x and y, with one grid node per ρ_s, and $2\pi qR$ in s with 16 grid nodes: $64 \times 256 \times 16$ nodes and a domain size of $64 \times 256 \times 2\pi$ in normalised units. This corresponds to basic parameters of $n_e = 4.6 \times 10^{13}\,\mathrm{cm}^{-3}$, $T_e = 130\,\mathrm{eV}$, $B = 20\,\mathrm{kG}$, $R = 165\,\mathrm{cm}$, $L_\perp = 2.5\,\mathrm{cm}$, $M_i/m_e = 4000$, $q = 3$ and a domain size of $2.5 \times 10\,\mathrm{cm}$ in the drift plane and 31 m along the magnetic field, all corresponding to typical edge parameters at the L-H transition in ASDEX Upgrade [23]. Note that this parameter regime ($\hat{\beta} > 1$, $\hat{\mu} > 1$, $\hat{\mu}\nu^2 \sim 1$) as noted in the Introduction is the result of the large size of $qR/L_\perp = 200$.

The temporal behaviour is shown in Fig. 1. This is the basis for the judgement that the turbulence is well saturated: the free energy levels, source/sink rates, and transport levels are statistically stationary after $t = 100$. Measurements taken over any interval of $\Delta t = 50$ between $t = 100$ and $t = 1000$ are consistent with each other within one standard deviation (see [21] for how these are defined and judged). For example, the average ExB thermal energy flux, Q_H, was 9.47 between $200 < t < 1000$, and for the $\Delta t = 50$ intervals ending at $t = 200$, 400, 600, 800, and 1000 it was 9.08, 10.0, 10.6, 8.42, and 9.00, respectively. This statistical variation is less than the difference between the levels at the different parameters used in the scaling results. This is a very rapid saturation compared to the two dimensional sheared slab model computations [21] but comparable to the electrostatic three dimensional models [22], a result of the fact that the drift wave nonlinear instability in general is much more robust in three dimensions than in two [44]. Other cases were not carried all the way to $t = 1000$; most needed only go to $t = 200$ and the weaker ones to $t = 300$. All cases were carried until at least the last $\Delta t = 100$ was saturated. Free energy and transport levels and source/sink rates were averaged over the last $\Delta t = 50$ and spectral and other mode structure information was averaged over the last $\Delta t = 100$.

The basic mode structure is shown in Fig. 2. It is the same as that observed in the electrostatic model [22], with the free energy peak at somewhat lower k_y than the $k_y\rho_s \sim 0.15$ peak in the source/sink rates. The important source/sink rates are the drift wave ones: ExB gradient drive and resistive, conductive, and Landau parallel electron dissipation ($\Gamma_n, \Gamma_t, \Gamma_c, \Gamma_k, \Gamma_l$). All of the source/sink rates peak together, but the source rate spectrum is narrower, indicating spectral transfer to both lower and higher k_y out of the net source region. Each state variable has its own cascade properties under ExB turbulence, with ExB energy going to lower k_y and n and T going to higher k_y, and each of these cascades operates indepently no matter what coupling regime the turbulence is in [60]. This is classic nonlinear drift wave mode structure, first observed in the two dimensional sheared slab model [28], discussed at length in [21], and shown to persist in tokamak geometry [22]. The vorticity spectrum is clean all the way to the last available mode, $k_{\max}\rho_s = 128 \times 0.025 \approx 3$, showing that the numerical scheme for ExB advection is well behaved. The flux surfave averaged source/sink rates exhibit only smooth, statistical variation with x, showing that there is no special effect of resonant surface layers, and that there is no pathology introduced by truncation in the y direction with respect to the parallel boundary condition.

The basic electromagnetic character of the turbulence is shown by its dependence on $\hat{\beta}$. All free energy and transport levels varied the same way, so it is sufficient to show only the transport, in Fig. 3. This and other scalings are in terms of time and space averages, over the full domain and over the last $\Delta t = 50$. The transport is almost entirely ExB transport, with magnetic flutter accounting for as much as a few percent of Q_H only for $\hat{\beta} = 20$. Particle magnetic flutter transport averaged over any substantial radial distance is essentially zero, since the same dependent variable is responsible for both $\tilde{\nabla}_{\|}$ and $J_{\|}$ [37]. The thermal energy transport due to magnetic flutter is small because the shorter and longer wavelengths tend to have different signs. At short wavelength, $q_{\|}$ and ψ have essentially no coherence, so that a simple random walk model is sufficient to explain the positive average magnetic flutter transport (it would be zero if ω_t were zero). But at long wavelength the Alfvén transit dynamics is faster than the turbulence, so it is nearly linear and therefore somewhat stabilising [18]. The magnetic flutter transport tends therefore to be negative at low k_y, and the average over the spectrum is very small.

Probabaility distributions for the amplitudes of ϕ, n, T, and the quantities directly measured by Langmuir probes [5–12], $I_{\rm sat} = n + \frac{1}{2}T$ and $\phi_{\rm fl} = \phi - 3T$, are shown in Fig. 4. The probability of a given variable having a given amplitude, A/σ in terms of standard deviations away from the mean, is shown as $P(A)$, compared to a perfect Gaussian distribution drawn with a dashed line. All of the $P(A)$ are essentially Gaussian, with negligible departures visible only at the level of several standard deviations. A similar signature was seen in all the various cases with differing $\hat{\beta}$, as well as those in which either magnetic curvature or magnetic flutter were removed from the equations. It would be

very difficult to argue in favor of coherent structure behaviour on the basis of the weak departures from perfect Gaussian distributions seen in this figure. The result is entirely consistent with conditional sampling experiments with Langmuir probes [10].

The cross coherence between n and ϕ, and between T and ϕ, is shown in Fig. 5, for $\hat{\beta} = 0.3$ (electrostatic, drift wave) and $\hat{\beta} = 10$ (electromagnetic, drift Alfvén wave). In such a measurement, each variable is sampled as for $P(A)$ above, and recorded as A/σ. In each case, each sample, taken at all 256 independent positions in the y direction, for various values of x in the vicinity of $x = 0$, and at $s = 0$. Each time point for each x and y position is one sample, so that the cross coherence is computed as the probability of finding both variables at a speficied ordered pair of amplitudes. The width of the contour ellipses away from the line on which the amplitudes are equal may be judged as the degree to which the two variables are incoherent with respect to one another. In the drift wave regime the coherence with ϕ is visible, slightly less for T than for n. Much of this is washed out at higher $\hat{\beta}$. By comparing the nominal case at $\hat{\beta} = 10$ with the one in which magnetic flutter was removed from the equations (linear $\nabla_{\parallel}$), we find that both the increased strength of the turbulence at the higher $\hat{\beta} = 10$ and the presence of magnetic flutter are concurrently responsible for the weakening of cross coherence with $\hat{\beta}$, a trend that was found to be monotonic. The apparently ubiquitous measurement of very weak cross correlation in Langmuir probe experiments [65] may be accounted for in part by these drift Alfvén electromagnetic effects.

The probability distribution for the phase shifts, shown in Fig. 6, add insight. In each case, the variable is sampled on a line of all 256 independent positions in the y direction, for various values of x in the vicinity of $x = 0$, and at $s = 0$. Each time point for each x position is one sample, for each wavenumber k_y from 0.025 to 3.2, and the probability of a variable to have a given phase shift, $\alpha \in [-\pi, \pi]$, in the y direction with respect to ϕ at that k_y is shown as $P(\alpha)$. In the electrostatic regime, here represented by $\hat{\beta} = 0.3$, both n and T are well ordered with respect to ϕ, such that the Gaussian distributions of their amplitudes seen in Fig. 4 are due to the same amplitude distribution of ϕ. This shows that the fact of a Gaussian distribution for a single state variable by itself is not sufficient to conclude that the turbulence is of the random mixing (passive scalar) type. With no coupling between n and ϕ, the distribution $P(\alpha)$ would be nearly random, with a general shift to positive values whose size depends on the relative strength of the gradient drive to the turbulent mixing. In the electrostatic regime the coupling of ϕ back towards $\widetilde{p} = n + T$ is very strong, especially at longer wavelength, so that the quantities being transported have a strong influence on how the ExB flow eddies are to subsequently evolve — this is the opposite of passive scalar turbulence. In the electromagnetic regime, here represented by $\hat{\beta} = 10$, the $P(\alpha)$ are both much broader; the reader can see the clear correspondence between the width of $P(\alpha)$ and the width of the cross coherence contour ellipses in Fig. 5. That much of this is due to small scale magnetic flutter is seen from the

differences between the nominal and linear $\nabla_{\|}$ cases for $\hat{\beta} = 10$. Magnetic flutter is able to randomise especially T with respect to ϕ at the smallest scales. However, in the energy producing range centered upon $k_y \rho_s = 0.15$ the contrast to what a randomised state would show is still quite visible. Together with the absence in Fig. 4 of the flattened tail in the amplitude distributions which would be expected in passive scalar dynamics [66], this leads to the conclusion that drift Alfvén turbulence is still reasonably well enough coupled that it would be difficult to model with a simple random mixing approach.

These fluctuation statistics show that although the amplitude distributions are all Gaussian, and although the magnetic flutter greatly reduces state variable cross coherence, the phase shift distributions are narrow enough to show that the turbulence is not of the random mixing or passive scalar type. On the other hand, there is no evidence of any behaviour which can be called coherent structure, even in the sense discussed in [21]. This is likely due to the fact that the turbulence is much stronger in three dimensions than in two [44] — even in the two dimensional sheared slab model, the degree of coherence had an inverse relationship to the turbulence strength (see the marginal amplitude threshold case discussed in [21]). Any coherent activity which slips past these diagnostics can be judged subtle enough not to have signicifant impact on the internal dynamics of the turbulence or on the transport level.

Finally, visual support for the foregoing is provided by the spatial morpholgy of the main state variables, shown in Fig. 7, along with the vorticity. Clear correlation among ϕ, n, and T is visible at the main eddy scale, relaxing at smaller scales as the turbulence is more effectively able to compete with the Alfvénic transients. Large radially streaming flows noted elsewhere [67] are not observed here as they are essentially prevented by the boundary conditions. No dipole vortices [68] are observed, either. While these features may be interesting in particular cases, neither is a necessary condition for robust turbulence and transport, or the nonlinear drift wave/drift Alfvén instability.

6. Results — Drift Alfvén or Ballooning?

The question arises, whether drift Alfvén, ballooning, or magnetic flutter physics (a tendency of $\nabla_\parallel J_\parallel$ to go to zero under a nonlinear magnetic response [61]) is responsible for the scaling with $\hat{\beta}$ and therefore the principal type of physics behind electromagnetic fluid drift turbulence. The simplest way to decide this is to apply a falsifiability check: if an agent is removed from the computation, its importance can be determined by the effect on the qualitative physical character (*e. g.*, rippling modes were found not to be important to drift wave turbulence in typical tokamak edge regimes by removing the rippling drive source and observing the total lack of an effect [50]). To this end, a scaling with $\hat{\beta}$ was obtained for three other situations: removing the curvature terms by setting $\omega_B = 0$ ("nocv"), removing the magnetic flutter by setting $\nabla_\parallel = \partial/\partial s$ ("nomag"), and removing both, such that only drift wave physics plus magnetic induction was left ("ind"). These were compared to the cases with all terms present ("main"). The $\hat{\beta}$ scalings are shown in Fig. 8. One can see that magnetic curvature is destabilising and magnetic flutter is stabilising, but that the scaling of Q_H with $\hat{\beta}$ is close to the same in all these cases. The slight differences in the shapes of these curves are explained by the varying strength of each effect in competition with the others: Magnetic curvature competes more strongly against weaker turbulence, so it has a strong quantitative effect on the transport level in the electrostatic regime [55], even when it introduces no qualitative change in the dynamics [22]. Additionally, as the ideal ballooning boundary is approached, $\mathcal{K}(p)$ begins to compete more effectively with $\hat{\beta}\nabla_\parallel^2(n + T - \phi)$ [38]. Magnetic flutter has an increasing effect with larger $\hat{\beta}$, so the "nomag" curve is steeper than the others at $\hat{\beta} = 10$. Obviously, if magnetic induction were additionally removed the curve would be horizontal, since $\hat{\beta}$ enters at all only through magnetic induction and flutter. The result is that the dependence of the turbulence on $\hat{\beta}$ is the result primarily of magnetic induction, and is therefore the result of the slowing down of parallel electron dynamics through the slower Alfvén velocity — the effect of electromagnetic character on this turbulence is the same as that observed in [36]. Like collisionality, it makes the electrons more nonadiabatic through slower parallel dynamics.

We learn more from this by looking for changes in the mode structure. Fig. 9 shows the changes in the total source (Γ_+) and sink (Γ_-) spectra due to the removal of the magnetic curvature and magnetic flutter terms. The removal of magnetic curvature shows that its effect was to add to the relative phases between n or T and ϕ; the result of removing is to decrease the size of Γ_+ but to leave the spectra unchanged. Magnetic flutter is significantly more important, in stabilising both the long and short wavelength sink regions as $\hat{\beta}$ increases; removing it causes a strong enough rise in Γ_+ that the extra strength of the turbulence can shift it to longer wavelength, through the ExB energy inverse cascade.

The changes in the cross coherence as a result of removing these effects are not as dramatic. Fig. 10 shows the cross coherence between n and ϕ as a function of $\hat{\beta}$ for each of the four series. Magnetic curvature has no effect, but magnetic flutter is part of the cause of the weakening cross coherence with rising $\hat{\beta}$. This is essentially how magnetic flutter helps stabilise the turbulence, and it is interesting as a signature which is possibly measurable by probe experiments. It is also interesting to note that magnetic flutter is the stronger of these two auxiliary effects.

Even weaker was the dependence of the phase shift probability distributions for n relative to ϕ due to these effects, shown in Fig. 11. In all cases, the role of the parallel dynamics in keeping these distributions much narrower than $\pi/2$ is dominant over all other effects. This is very basic, because it is the principal signature of the self-consistency which causes the turbulence to differ from the random mixing type.

This tells us something important: the basic physical character of the turbulence has nothing to do with ballooning, ideal or otherwise. Magnetic curvature causes ballooning by increasing the phase shift between $p = n + T$ and ϕ where it is unfavorable ($\cos\theta > 0$) and decreasing the phase shift where it is favorable ($\cos\theta < 0$), but this is an additional perturbation on an already established drift Alfvén turbulence. In no case was curvature observed to alter the qualitative mode structure or cross coherence, even when curvature had a very strong quantitative effect. This has been noted before in drift wave physics, in both the two dimensional sheared slab [62] and three dimensional tokamak geometry [22] models. It is a very robust result. That magnetic flutter affects the qualitative mode structure more than does curvature adds to the emphasis.

The main result of this section is that the conclusion that three dimensional elctron fluid turbulence at tokamak edge parameters is drift wave turbulence [22] is not changed by the introduction of transcollisional or electromagnetic physics; it is merely generalised to drift Alfvén turbulence. The principal electromagnetic effect is magnetic induction, leaving the physical character of two dimensional ExB drift plane turbulence coupled by parallel electron dynamics unchanged, with magnetic flutter the most important auxiliary effect. The scaling of the turbulence and transport with $\hat{\beta}$ is the result of the slower Alfvén parallel dynamics at larger $\hat{\beta}$. The salient parameter is $\hat{\beta}$ because it gives the square of the ratio of the basic drift frequency, $c_s/L_\perp$, to the Alfvén transit frequency, v_A/qR.

7. Results — Scaling with Parameters Other Than Beta

This section presents the rest of the parametric dependence of drift Alfvén turbulence and transport. Except for magnetic shear, no scaling is as pronounced as the one with $\hat{\beta}$. A scaling against the temperature gradient holding the pressure gradient fixed shows that the turbulence is roughly equally well driven by either ∇n or ∇T, with the total drive and heat flux somewhat larger when $\nabla p \to n\nabla T$. Scaling against ν is very weak for $\nu < 0.5$ and not nearly so strong as in collisional electrostatic models even for $\nu \gtrsim 1$. The most important parameter is therefore $\hat{\beta}$, consistent with the characterisation of the turbulence as drift Alfvén turbulence.

The most important of the auxiliary parameters is the collisionality. For electrostatic drift waves, the collisional parameter is $C_0 = (\nu_e L_\perp / c_s)(m_e/M_i)(qR/L_\perp)^2 = \hat{\mu}\nu$; it controls the relative speed of the parallel electron dynamics in damping force imbalances and enforcing an adiabatic state. Previous work with both the two dimensional sheared slab [21] and three dimensional models [22,55] models has shown a very strong dependence of the turbulence and transport level with C_0, due to the fact that the strength of the nonlinear instability [21,28] depends recursively on the amplitude of the turbulence. The scaling of drift Alfv'en turbulence at $\hat{\beta} = \hat{\mu} = 10$, however, is much weaker, as can be seen in Fig. 12. The speed parallel dynamics is controlled not by C_0 but by $\hat{\beta}$, so that the scaling of the turbulence and transport is much more sensitive to $\hat{\beta}$ than to ν. For $\nu = 0.5$ the collisional damping of $J_\parallel$ and $q_\parallel$ is comparable to the Landau damping of $q_\parallel$, as seen in Fig. 2. For $\nu < 0.5$ the collisions are weaker and the principal dissipation mechanism is Landau damping; the scaling in this regime with ν is very weak. As ν is increased above 0.5, collisional dissipation begins to take over, starting at the smaller wavelengths and moving into the spectrum towards the energetics peak at $k_y\rho_s = 0.15$. The turbulence is stronger with larger ν for the same reasons as in the collisional, electrostatic drift wave model: the parallel response is slowed down. But at least as far as $\nu = 2$ the scaling is still weaker than that for $\hat{\beta}$. In experimental terms, however, an increase of the total heat transport of a factor of two is very important, perhaps enough to affect the state of the tokamak edge. More discussion of this appears in Section 8.

The other auxiliary parameter is the curvature, controlled by $\omega_B = 2L_\perp/R$. This determines the relative strength of interchange and ballooning dynamics; indeed, the MHD ballooning parameter is proportional to $\hat{\beta}\omega_B$ [40,59]. Although we have already seen that ω_B is too weak to change the qualitative character of the turbulence, it is still important quantitatively. The scaling of the transport level with ω_B for $\hat{\beta} = \hat{\mu} = 10$ appears in Fig. 13. For $\omega_B < 0.03$, its nominal value, there is little variation of q_H with ω_B, although again a change of 30 percent can be important experimentally. As ω_B is increased above 0.05, the curvature's quantitative effect becomes pronounced, especially as the ideal ballooning limit (about 0.15) is approached. Although the computations could not be extended into the

ballooning regime for numerical reasons, it is to be expected that a fundamental change occurs there due to the destabilisation of the entire spectrum, possibly at wavelengths even longer than those kept in these computations ($\lambda_{\max} = 256\rho_s \sim 10\,\mathrm{cm}$, corresponding to a poloidal mode number of about 60 in ASDEX Upgrade). Whether the boundary is a hard one remains to be seen (especially if two fluid effects are kept in ballooning stability calculations [38]), but the distribution of observed edge states in ASDEX Upgrade (Section 8) suggests it is. However, it is important to note that even for $\omega_B = 0.1$ the qualitative as opposed to quantitative effect was negligible.

Another important feature of thermal gradient driven turbulence is the extent to which it is dependent on each of the gradients present (in this case, ∇n and $\nabla T_e \to \nabla T$). Drift waves especially are thought of as ∇n driven modes, and when ∇T is thought to be experimentally important, people often begin a search for other types of mode [3]. However, either of these two gradients can drive even electrostatic drift wave turbulence, and ∇T drives it even more strongly than does ∇n (see [21] or [22]; note, though, that a stronger drive by ∇T does not always correspond to stronger turbulence, as more conductive dissipation can be excited [63]). Fig. 14 shows the dependence of the transport level on the $\Delta_T = d\log T/d\log p = \omega_t/(\omega_n + \omega_t)$ of the profile, with the profile $\nabla p = \omega_n + \omega_t \to 2$ held constant. The ExB drives, Γ_n and Γ_t vary as one might expect, and at the nominal case of $\Delta_T = 0.5$ the excess of Γ_t over Γ_n is due mostly to the factor of 3/2 in Eq. (21). The proportion of the drive due to ∇n and ∇T is thus much more even than in the electrostatic case (see [22], in which Γ_t was about 4 times Γ_n for $\omega_n = \omega_t$), due possibly to the weaker cross correlation in the electromagnetic regime. The total transport, however, is only weakly dependent on Δ_T, varying by at most 50 percent over the entire range. It is therefore clear, that drift Alfvén turbulence is driven by the total thermal gradient, and is important whether or not the density or temperature profile is flat. A similar result was also obtained in the first electrostatic computations with all three of ϕ, n, and T as state variables [22].

Finally, the magnetic shear, S, the sensitivity of the transport to which is shown in Fig. 15. There is a relatively strong dependence on shear for $S \gtrsim 0.5$, due to the effect shear has on the structure of a disturbance of the flux tube type: as one moves down the magnetic field lines, the distance between two points on different field lines increases in the y direction, leading to the coordinate deformation implicit in Eq. (18) and therefore a stronger tendency for flux tube like structures to break up in the parallel direction [64]. The shorter parallel correlation length in turn leads to slightly more adiabatic electrons — for $S = 0.1$ the set $\{\Gamma_n, \Gamma_t, \Gamma_c, \Gamma_k, \Gamma_l\}$ was $\{4.10, 6.51, 1.19, 2.38, 1.29\} \times 10^{-2}$, and for $S = 1.0$ it was $\{3.16, 5.82, 1.41, 2.29, 1.35\} \times 10^{-2}$. The largest change was actually in the drive. For $S > \gtrsim 0.5$ the correlation length drops below $2\pi qR$ and is therefore approximately inversely proportional to the shear, much as seen in much more simplified computations [64] (this conclusion follows as well from two dimensional sheared slab analysis [21]). This would explain the apparent break in the curves of transport level as functions of S.

8. Applicability to the L-H Transition in Tokamaks

Under auxiliary heating, the tokamak edge region is observed to abruptly change its state [1], from one characterised by a cooler edge and a thermal gradient smoothly varying from near edge to edge, to one with a higher edge temperature and a steep gradient region of some cm inside the last closed flux surface within which the temperature can change by as much as a factor of four [69]. These are called the L-mode and H-mode states, respectively, since they have relatively lower and higher confinement properties. The parameters in this edge region are of interest because they indicate which types of physics may be prominently active in the turbulence and transport occurring there. An example from the ASDEX Upgrade tokamak is shown in Fig. 16 [23] (see also [70]). Several observed states are plotted in terms of the temperature and density measured 2 cm inside the last closed flux surface, within the steep gradient region. The L- and H-mode states are judged according to the criteria which describe an H-mode. It is seen that there is a transition boundary, which depends mostly on this near edge temperature (and also on the magnetic field), and more weakly on the density — at higher densities the density dependence disappears [29,71,72], leading to the suggestion that collisional physics may be at play [73]. It is observed that no states occur within the two grey zones. The upper one scales with β and is interpreted as the ideal ballooning regime. The lower one is characterised by the presence of radiation instabilities. Also plotted on Fig. 16 are lines indicating the $\nu = 0.5$ boundary, above which the drift Alfvén turbulence is at most marginally collisional, and the $\hat{\beta} = 1$ boundary, above which the electron response is electromagnetic — this is the separator between the drift Alfvén and drift wave regimes. The $\beta = m_e/M_i$ line is also shown, noting its proximity to the actual line of the L-H transition [39]. It is seen that almost all of the states lie within the transcollisional drift Alfvén regime: $\hat{\beta} > 1$, $\nu < 0.5$, and stable to ideal ballooning. Although there is significant quantitative effect due to ballooning physics throughout the drift Alfvén regime as shown in Sections 5 and 6, the ideal ballooning regime is different because much longer wavelength MHD modes are destabilised there. This is quite different from the ballooning found in these drift Alfvén computations, in which no qualitative changes due to magnetic curvature were found.

We are left with a dilemma: if drift Alfvén dynamics has this obvious a role in the L-H transition, how is the fact that the transport rises so sharply with $\hat{\beta}$ to be reconciled with the observations that local transport should improve when the H-mode is entered? The answer certainly lies in the physics of the interaction between the profiles and the turbulence, which has not been considered here. Preliminary computations with a nonlocal electrostatic model have shown that nonlocal and local physics can be very different quantitatively if the background conditions vary appreciably over a few typical ExB eddy

widths [22], most especially near the last closed flux surface where there is strong interaction with the scrape off layer, characterised by open field lines bounded by Debye sheaths [11,22,74]. Especially ExB spin up physics [75,76] has not been considered here (intentionally, in fact, due to the small extent of the computational domain in the x direction). A nonlocal computation (now under construction) will be needed to properly address this.

The bottom line is that drift Alfvén dynamics are of certain relevance to the L-H transition, but the interaction between turbulence and profiles, especially the prospect that there may be no practical difference between the two, will have to be investigated before anything can be claimed about an L-H transition computation.

9. Conclusions

The dynamics of passing (non-trapped) electrons in turbulence is completely dominated by nonlinear dynamics, as is already known from electrostatic work [21,22], and as this paper has now shown for drift Alfvén turbulence. This makes the conclusions of linear stability theory as irrelevant as they were in the case of the two dimensional sheared slab model [21,50]. Drift Alfvén turbulence is strongly influenced by electromagnetic induction for $\hat{\beta} > 1$ and totally dominated by it by the time $\hat{\beta} > \hat{\mu}$, or equivalently $\beta > \mu_e \equiv m_e/M_i$. The principal effect of magnetic induction is to slow down the parallel electron dynamics through a slower Alfvén velocity; magnetic flutter (the perturbed $\nabla_\parallel$) has an auxiliary role to diminish state variable cross coherence, and magnetic curvature has a role which is qualitatively even weaker: to increase the average phase shifts between n or T and ϕ already established by the drift Alfvén turbulence. Although there are a lot of effects which can effect the experimental situation, including magnetic flux surface geometry, ExB profile dynamics, and interaction with neutrals, the nonlinear drift Alfvén turbulence is so robust that these can be expected to have only quantitative effects — they will be needed for detailed comparison to experiment, but they are not needed to understand the underlying physics.

This goes particularly for ballooning effects. It is already known that even when magnetic curvature can dominate the linear behaviour and greatly increase the strength of turbulence, in both the two dimensional sheared slab [62] and three dimensional electrostatic, collisional [22,55] models, its effect on turbulence is purely quantitative, without important changes in the basic character [22,62]. That result is confirmed here in both the electrostatic and drift Alfvén limits. The effect of curvature on the energy and source/sink spectra and on cross coherence is found to be negligible, even when the quantitative effect of curvature on the turbulence level is strong. The scaling with $\hat{\beta}$ is likewise unaffected. This shows unequivocally that the underlying dynamics is drift Alfvén and not ballooning mode dynamics. The only outstanding effect in the general electron drift dynamics to be checked is magnetic trapping, but this will have to be studied with a kinetic model to yield a definitive result.

Although the parametric limit beyond which the turbulence becomes electromagnetic ($\hat{\beta} > 1$) is much the same as in the previous two dimensional study [36], the effect in three dimensions is to make the turbulence stronger, not weaker. This follows together with the effect of collisionality: both $\hat{\beta}$ and ν enter to slow down parallel electron dissipation and thereby allow the turbulence to be stronger, because slower parallel electron dynamics means weaker coupling between n or T and ϕ. The nonlinear fluid drift instability in three dimensions is similar to the two dimensional sheared slab version [22], but both are completely different from the two dimensional homogeneous situation [21,44]. In this work it is clear that both increased $\hat{\beta}$ and increased ν lead to stronger turbulence and transport,

although $\hat{\beta}$ has more influence. The basic nonlinear instability at work is the drift wave version, and the principal effect of finite beta is for magnetic induction to slow down the parallel electron dynamics and thereby make that nonlinear instability stronger.

No tendency to form coherent structure or structures of any sort, neither vortices [68] nor the sort of preferential phase relations or non-Gaussian statistics which were observed in the two dimensional sheared slab model [21] was observed for this three dimensional turbulence . Amplitude distributions were found to be Gaussian within the numerical statistical limits (*i. e.*, to at least 2 to 3 standard deviations). The magnetic nonlinearity has a weak randomising influence, but so also does magnetic induction by itself, through the stronger ExB turbulence to which it leads. However, the phase shift probability distributions showed the turbulence still to be too well coupled to be describable by random mixing pr passive scalar dynamics. The evolution of the ExB eddies is still self consistently determined by parallel dynamics.

Two interesting results are that the strong scaling with ν seen in drift wave computations [21,22,55] disappears in the drift Alfvén regime, and that the total thermal energy transport is not very sensitive to which gradient (∇n or ∇T_e) drives the turbulence. Both of these are consistent with a detailed experimetal study whose aim it was to determine the type of turbulence from a large database of Langmuir probe measurements [9]. This improves the correspondence of the computational results to actual experimental findings.

In conclusion, then, the basic physics of fluid drift electron turbulence in a strongly magnetised plasma is drift Alfvén turbulence, whose electrostatic ($\hat{\beta} < 1$) limit is drift wave turbulence.

References

[1] Initial discovery and reviews of the L- and H-mode phenomenon: F. Wagner, *et al*, *Phys. Rev. Lett.* 49 (1982) 1408; The ASDEX Team, *Nucl. Fusion* 29 (1989) 1959; R. J. Groebner, *Phys. Fluids B* 5 (1993) 2343.

[2] P. C. Liewer, *Nucl. Fusion* 25 (1985) 543.

[3] A. J. Wootton, B. A. Carreras, H. Matsumoto, K. McGuire, W. A. Peebles, Ch. P. Ritz, P. W. Terry, and S. J. Zweben, *Phys. Fluids B* 2 (1990) 2879.

[4] M. Bessenrodt-Weberpals, F. Wagner, ASDEX Team, ICRH Team, LH Team, NI Team, Pellet Injection Team, PSI Group, O. Gehre, L. Giannone, J. V. Hoffmann, A. Kallenbach, K. McCormick, V. Mertens, H. D. Murmann, F. Ryter, B. Scott, G. Siller, F. X. Söldner, A. Stäbler, K.-H. Steuer, U. Stroth, N. Tsois, H. Verbeek, and H. Zohm, *Nucl. Fusion* 33 (1993) 1205.

[5] W. L. Rowan, C. C. Klepper, Ch. P. Ritz, R. D. Bengston, K. W. Gentle, P. E. Phillips, T. L. Rhodes, B. Richards, and A. J. Wootton, *Nucl. Fusion* 27 (1987) 1105.

[6] Ch. P. Ritz, D. L. Brower, T. L. Rhodes, R. D. Bengston, S. J. Levinson, N. C. Luhmann, Jr., W. A. Peebles, and E. J. Powers, *Nucl. Fusion* 27, 1125 (1987).

[7] Ch. P. Ritz, E. J. Powers, and R. D. Bengston, *Phys. Fluids B* 1, 153 (1989).

[8] Ch. P. Ritz, R. V. Bravanec, P. M. Schoch, R. D. Bengston, J. A. Boedo, J. C. Forster, K. W. Gentle, Y. He, R. L. Hickok, Y. J. Kim, H. Lin, P. E. Phillips, T. L. Rhodes, W. L. Rowan, P. M. Valanju, and A. J. Wootton, *Phys. Rev. Lett.* 62 (1989) 1844.

[9] T. L. Rhodes, Ch. P. Ritz, and R. D. Bengston, *Nucl. Fusion* 33 (1993) 1147.

[10] A. V. Filippas, R. D. Bengston, G.-X. Li, M. Meier, Ch. P. Ritz, and E. J. Powers, *Phys. Plasmas* 2 (1995) 839.

[11] M. Endler, H. Niedermeyer, L. Giannone, E. Holzhauer, A. Rudyj, G. Theimer, N. Tsois, ASDEX Team, *Nucl. Fusion* 35 (1995) 1307.

[12] C. Hidalgo, *Plasma Phys. Contr. Fusion* 37 (1995) A53.

[13] A.J. Wootton, R. Bengtson, R.V. Bravenec, J. Chen, G. Cima, P.H. Edmonds, M. Freeman, H. Gasquet, K. Gentle, G. Hallock, Y. Karzhavin, S. McCool, D. Patterson, P. Phillips, B. Richards, D. Roberts, W. Rowan, D. Ross, E. Solano, D. Sing, R.F.

Steimle, H. Tsui, J. Uglum, Y. Wen, Z. Zhang, R.F. Gandy, T.D. Rempel, M. Kwon, C. Watts, R. Durst, R.J. Fonck, D.L. Brower, Y. Jiang, W.A. Peebles, J.W. Heard, R.L. Hickock, A. Ouroua, P.M. Schoch, K.A. Connor, and G. Giruzzi, in *Plasma Physics and Controlled Nuclear Fusion Research 1994* (IAEA, Vienna 1995), Vol. 2, p. 73.

[14] S. S. Moiseev and R. Z. Sagdeev, *Sov. Phys. JETP* 17 (1963) 515.

[15] S.-T. Tsai, F. W. Perkins, and T. H. Stix, *Phys. Fluids* 13 (1970) 2108.

[16] F. L. Hinton and C. W. Horton, Jr, *Phys. Fluids* 14 (1971) 116.

[17] A. B. Mikhailovskii and L. I Rudakov, *Sov. Phys. JETP* 17 (1963) 621. See also J. T. Tang and N. C. Luhmann, Jr., *Phys. Fluids* 19 (1976) 1935, for a very clear exposition.

[18] P. J. Catto, A. M. El Nadi, C. S. Liu, and M. N. Rosenbluth, *Nucl. Fusion* 14 (1974) 405.

[19] A. Hasegawa and K. Mima, *Phys. Rev. Lett.* 39 (1977) 205; *Phys. Fluids* 21 (1978) 87.

[20] M. Wakatani and A. Hasegawa, *Phys. Fluids* 27 (1984) 611.

[21] B. Scott, *Phys. Fluids B* 4 (1992) 2468.

[22] B. Scott, in *Proceedings of the 22th European Conference on Controlled Fusion and Plasma Physics, Bournemouth, 1995* (European Physical Society, Bournemouth, 1995), p. I-229, shows functioning of collisional drift wave turbulence (CDWT) with zero density gradient; *Plasma Phys. Contr. Fusion* , Apr 97, shows three dimensional turbulence is CDWT, with no qualitative effect from ballooning.

[23] M. Kaufmann, J. Schweinzer, and the ASDEX Upgrade Teams, 16th IAEA Montreal, 1996, (to appear by IAEA, Vienna, 1997), paper O1-5.

[24] J. D. Callen, *Phys. Rev. Lett.* 39 (1977) 1540.

[25] J. Neuhauser, W. Schneider, and R. Wunderlich, *Nucl. Fusion* 26 (1986) 1679.

[26] A. Thyagaraja, UKAEA Culham Laboratory, Report FUS 303 (ISBN 0-85311-189-8), 1995.

[27] Bounce averaged fluid electron models: F. Y. Gang and P. H. Diamond, *Phys. Fluids B* 2 (1990) 2976; M. A. Beer and G. W. Hammett, *Phys. Plasmas* 3 (1996) 4018.

[28] B. Scott, *Phys. Rev. Lett.* 65 (1990) 3289.

[29] A. E. Hubbard, J. A. Goetz, M. Greenwald, I. H. Hutchinson, Y. In, J. Irby, B. Labombard, P. J. O'Shea, J. A. Snipes, P. C. Stek, Y. Takase, S. M. Wolfe, and the Alcator Group, 16th IAEA Montreal, 1996, (to appear by IAEA, Vienna, 1997), paper AP2-11.

[30] A. Hasegawa and L. Chen, *Phys. Fluids* 19 (1976) 1924.

[31] The first transcollisional drift wave turbulence computation, in the two dimensional sheared slab model and still using $k_{\|}$ as a parameter, appears in B. Scott, in *Proceedings of the 20th European Conference on Controlled Fusion and Plasma Physics, Lisbon, 1993* (European Physical Society, Lisbon, 1993), p. IV-1411. The nonlinear instability was shown to exist in the collisionless universal mode regime.

[32] A preliminary electromagnetic computation in the two dimensional slab model appears in B. Scott, in *Proceedings of the 21th European Conference on Controlled Fusion and Plasma Physics, Montpellier, 1994* (European Physical Society, Montpellier, 1994), p. II-560.

[33] G. Hammett and F. Perkins, *Phys. Rev. Lett.* 64 (1990) 3019.

[34] M. A. Beer and G. W. Hammett, *Phys. Plasmas* 3 (1996) 4046.

[35] K. Molvig, S. P. Hirshman, and J. C. Whitson, *Phys. Rev. Lett.* 43 (1979) 582.

[36] S. Camargo, B. Scott, and D. Biskamp, *Phys. Plasmas* 3 (1996) 3912.

[37] R. E. Waltz, *Phys. Fluids* 28 (1985) 577.

[38] J. D. Callen and C. C. Hegna, University of Wisconsin, Report UW-CPTC 96-5, August 1996.

[39] B. Scott, S. Camargo, and F. Jenko, 16th IAEA Montreal, 1996, (to appear by IAEA, Vienna, 1997), paper DP-18.

[40] B. Rogers, J. F. Drake, Y. T. Lau, P. N. Guzdar, A. B. Hassam, and S. V. Novakovski, 16th IAEA Montreal, 1996, (to appear by IAEA, Vienna, 1997), paper D1-4.

[41] D. Biskamp, E. Schwarz, J. F. Drake, *Phys. Rev. Lett.* 75 (1995) 3850.

[42] H. Strauss, *Phys. Fluids* 19 (1976) 134.

[43] J. F. Drake and T. M. Antonsen, Jr., *Phys. Fluids* 27 (1984) 898.

[44] D. Biskamp and A. Zeiler, *Phys. Rev. Lett.* 74 (1995) 706.

[45] S. I. Braginskii, *Rev. Plasma Phys.* 1 (1965) 205.

[46] A. B. Hassam, *Phys. Fluids* 23 (1980) 38.

[47] A. H. Boozer, *Phys. Fluids B* 4 (1992) 2845.

[48] B. B. Kadomtsev and O. P. Pogutse, *Rev. Plasma Phys.* 5 (1970) 296.

[49] H. P. Furth, J. Killeen, and M. N. Rosenbluth, *Phys. Fluids* 6 (1963) 459. See also B. Scott and A. B. Hassam, *Phys. Fluids* 30 (1987) 90, for the case with nonlinear tearing modes with temperature physics.

[50] B. Scott, *Nucl. Fusion* 32 (1992) 873.

[51] Evidence against anomalous resistivity in tokamaks: D. V. Bartlett, R. J. Bickerton *et al*, the JET Team, *Nucl. Fusion* 28 (1988) 73; M. C. Zarnstorff, K. McGuire, M. G. Bell, B. Grek, D. Johnson, D. McCune, H. Park, A. Ramsey, and G. Taylor, *Phys. Fluids B* 2 (1990) 1852.

[52] B. A. Carreras, L. Garcia, and P. H. Diamond, *Phys. Fluids* 30 (1987) 1388.

[53] K. Itoh, S.-I. Itoh, M. Yagi, A. Fukuyama, and M. Azumi, *Plasma Phys. Contr. Fusion* 36 (1994) 1501.

[54] K. V. Roberts and J. B. Taylor, *Phys. Fluids* 8 (1965) 315.

[55] A. Zeiler, D. Biskamp, J. F. Drake, P. N. Guzdar, *Phys. Plasmas* 3 (1996) 2951.

[56] R. L. Dewar and A. H. Glasser, *Phys. Fluids* 26 3038 (1983).

[57] M. A. Beer, S. C. Cowley, and G. W. Hammett, *Phys. Plasmas* 2 (1995) 2687.

[58] K. T. Tsang, J. C. Whitson, J. D. Callen, P. J. Catto, and J. Smith, *Phys. Rev. Lett.* 41 (1978) 557.

[59] J. W. Connor, R. J. Hastie, and J. B. Taylor, *Phys. Rev. Lett.* 40 (1978) 396.

[60] B. Scott, H. Biglari, P. W. Terry, and P. H. Diamond, *Phys. Fluids B* 3 (1991) 51.

[61] P. H. Rutherford, *Phys. Fluids* 16 (1973) 1903.

[62] B. Scott, in *Plasma Physics and Controlled Nuclear Fusion Research 1992* (IAEA, Vienna 1993), Vol. 2, p. 203.

[63] B. Scott, *Plasma Phys. Contr. Fusion* 34 (1992) 1977.

[64] A. Zeiler, D. Biskamp, and J. F. Drake, *Phys. Plasmas* 3 (1996) 3947.

[65] H. Niedermeyer, R. Balbin, J. Bleuel, M. Endler, L. Giannone, H. J. Hartfuß, M. Häse, G. Theimer, and C. Watts, "Fluctuations, Turbulent Transport, and Analysis Tools," presented at the Transport in Fusion Plasmas Workshop, Varenna, Sep 1996.

[66] Ya. G. Sinai and V. Yakhot, *Phys. Rev. Lett.* 63 (1990) 1962.

[67] J. F. Drake, A. Zeiler, and D. Biskamp, *Phys. Rev. Lett.* 75 (1995) 4222.

[68] Dipole vortex treatments: M. Kono and E. Miyashita, *Phys. Fluids* 31, 326 (1988). J. D. Meiss and W. Horton, *Phys. Fluids* 26 (1983) 990.

[69] Detailed pedestal profile measurements from D-III-D: P. Gohil, K. H. Burrell, E. J. Doyle, R. J. Groebner, J. Kim, and R. P. Seraydarian, *Nucl. Fusion* 34 (1994) 1057.

[70] H. Zohm, W. Suttrop, H. J. de Blank, R. J. Buttery, D. Gates, J. Hekkinen, W. Herrmann, A. Kallenbach, T. Kass, M. Kaufmann, T. Kurki-Suonio, B. Kurzan, M. Maraschek, H. Reimerdes, F. Ryter, H. Salzmann, J. Schweinzer, J. Stober, and the ASDEX Upgrade, ECRH, ICRH, and NBI Teams, 16th IAEA Montreal, 1996, (to appear by IAEA, Vienna, 1997) paper A5-1.

[71] R. J. Groebner, T. S. Carlstrom, K. H. Burrell *et al*, 16th IAEA Montreal, 1996, (to appear by IAEA, Vienna, 1997) paper AP2-10.

[72] E. Righi, A. Bickley, D. J. Campbell *et al*, Dedicated ITER H-Mode Power Threshold Experiments in JET, submitted to *Plasma Phys. Contr. Fusion* (1997).

[73] A. V. Chankin, "Critical Parameters for Turbulent Transport in the SOL: Mechanism for the L-H Transition and its Impact on the H-mode Power Threshold and Density Limit in ITER," submitted to *Plasma Phys. Contr. Fusion* (1997).

[74] A. V. Nedospasov, *Sov. J. Plasma Phys.* 15 (1989) 659.

[75] P. H. Diamond and Y. B. Kim, *Phys. Fluids B* 3 (1991) 1626.

[76] J. F. Drake, J. M. Finn, P. N. Guzdar, V. Shapiro, V. Shevchenko, F. Waelbroeck, A. B. Hassam, C. S. Liu, and R. Sagdeev, *Phys. Fluids B* 4 (1992) 488.

[77] P. Colella, *J. Comput. Phys.* 87 (1990) 171.

[78] R. D. Richtmeyer and K. W. Morton, *Difference Methods for Initial-Value Problems*, 2nd Ed (Wiley, New York, 1967), p 303. The predictor was chosen slightly overstable to prevent growth of small-scale waves in the parallel direction.

A. Numerical Methods

The scheme used to advance the equations is a collection of standard methods. ExB advection uses the multidimensional second order characteristic method of Colella [77]. The parallel dynamics uses a second order Crank Nicholson predictor corrector scheme [78]. The remaining effects are drive terms acting on slower time scales, and are evaluated explicitly at the current time step. The magnetic nonlinearities, the contribution of ψ to $\nabla_\parallel$, deserve comment. In the predictor step $\nabla_\parallel = \partial/\partial s - \hat{\beta}\mathrm{b}\times\nabla\psi \cdot \nabla$ is evaluated explicitly. In the corrector step the fluxes are set up conservatively, and here the evaluation is at points along the perturbed field lines. Given the predicted flux field defined at $s_{k+1/2}$ midway between s_k and s_{k+1} for each x_i and y_j, the field line passing through (x_i, y_j, s_k) is extended to $s_{k+1/2}$ at different (x, y) using $\hat{\beta}\psi$. Then, the divergence is evaluated in the usual way.

Figures

Fig. 1. Temporal evolution of the ExB energy (E_e), ∇T ExB drive (Γ_t), and ExB thermal energy flux (Q_H), showing saturation beyond about $t = 100$ for the nominal case.

Fig. 2. Typical drift wave and drift Alfvén mode structure. Energy spectra are shown for the ExB (E), density (n), temperature (T), sound wave (u), magnetic plus current (B), and parallel heat flux (q) contributions. Also shown is 10^2 times the vorticity spectrum (W). Spectra and spatial profiles are shown for the five drift wave source (n and T) and sink processes (c, k, and L). Spatial profiles are shown for the fluctuation amplitudes of ϕ, n, T, $u_\parallel$, $J_\parallel$, and $q_\parallel$. Noteworthy features are pointed out in the text.

Fig. 3. Scaling with $\hat{\beta}$ of the ExB and magnetic flutter contributions to the particle and thermal energy transport. Transport is due to ExB eddies, and the drift Alfvén regime is $\hat{\beta} \gtrsim 1$.

Fig. 4. Amplitude probability distribution functions in terms of standard deviations away from the mean, for the state variables (ϕ, n, and T) and the two derived quantities most often measured by Langmuir probes (I_{sat} and ϕ_{fl}). Departures from a Gaussian distribution (dashed lines) are small, and the distributions are closer to Gaussian than to a passive scalar distribution (dotted lines).

Fig. 5. Cross coherence between n or T and ϕ for the nominal case ($\hat{\beta} = 10$), compared to the electrostatic case ($\hat{\beta} = 0.3$) and one without magnetic flutter (linear $\nabla_\parallel$). The tight coherence in the drift wave regime is relaxed in the drift Alfvén regime, partly due to magnetic flutter.

Fig. 6. Lest the previous two figures motivate a random mixing turbulence model, the probability distributions of the phase shift of n or T ahead of ϕ are shown for each k_y, for the three cases of Fig. 5. The drift wave case is the most strongly coupled, but even the drift Alfvén case is too well ordered for a passive scalar model. Though magnetic flutter tends to randomise the phases, ϕ is still sensitive to both n and T in the energy producing range ($0.1 < k_y < 0.3$).

Fig. 7. Spatial distribution of the main state variables and the vorticity, showing ExB eddies in strong turbulence, well coupled to the quantities (n and T) they are transporting. The vorticity is clean down to the grid scale, as its spectrum (Fig. 2) indicates.

Fig. 8. Case series with the removal of magnetic curvature (no curv), magnetic flutter (no mag), or both (ind), have the same basic scaling with $\hat{\beta}$ as the nominal series (main), showing that magnetic induction is the principal electromagnetic effect.

Fig. 9. Total source (Γ_+) and sink (Γ_-) spectra for the four cases of Fig. 8, at $\hat{\beta} = 10$. The basic stabilising effect of magnetic flutter and destablising effect of magnetic curvature on the source rates is visible, as is the lack of qualitative effect due to curvature alone.

Fig. 10. Cross coherence between n and ϕ for the four cases of Fig. 9, showing the moderate decorrelation effect of magnetic flutter and the weak signature of magnetic curvature.

Fig. 11. Phase shift probability distributions for n relative to ϕ for the four cases of Fig. 9, showing that the non-random nature of the turbulence is not appreciably altered by the presence or absence of magnetic curvature or flutter. The dotted lines are drawn through the $k_y \sim 0.15$ energetic maximum of the nominal case, and $\alpha = 0$.

Fig. 12. Scaling of the nominal case with collisionality, showing the weak dependence of the ExB transport for $\nu < 0.5$ but the increasing importance of ν above 0.5. Magnetic flutter transport is insensitive to ν and small. The vertical scale is linear, and the horizontal scale if logarithmic except for the $\nu = 0$ case.

Fig. 13. Scaling of the nominal case with magnetic curvature, showing the weak dependence at the nominal value $\omega_B = 2L_\perp/R = 0.03$, but a much stronger dependence as the ideal ballooning limit (about 0.15) is approached.

Fig. 14. Scaling of the nominal case with $d\log T/d\log p$ of the profile, holding the total ∇p fixed, showing that both ∇n and ∇T drive the turbulence in proportion to their relative strength, with ∇T somewhat greater due to the factor of 3/2. Drift Alfvén transport remains effective when either profile becomes flat, so that the total thermal gradient is the overall source of free energy.

Fig. 15. Scaling of the nominal case with magnetic shear. The break at $S \approx 0.5$ occurs when shear takes over from the finite connection length in determining the parallel scale.

Fig. 16. Diagram of near edge parameters for most of the L-H transition database in ASDEX Upgrade. Temperature and density, both measured 2 cm inside the separatrix, are plotted against each other. The $\hat{\beta} = 1$ and $\nu = 0.5$ lines together with the ideal ballooning boundary enclose the transcollisional drift Alfvén regime, which is seen to occupy most of the operation space.

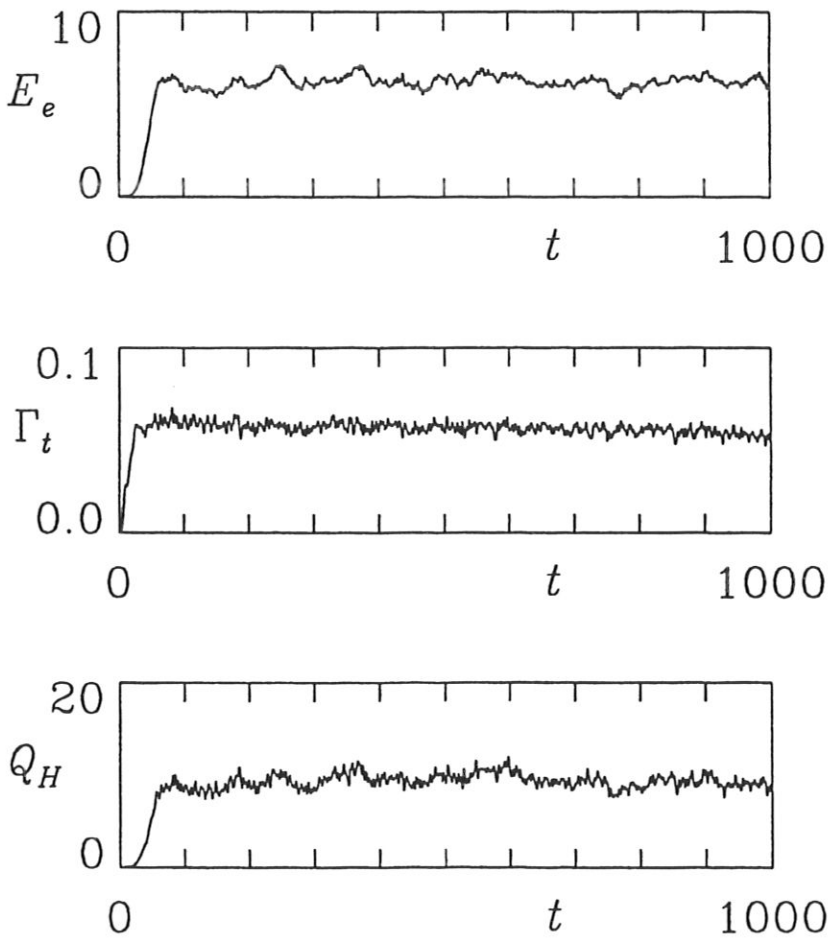

Fig I

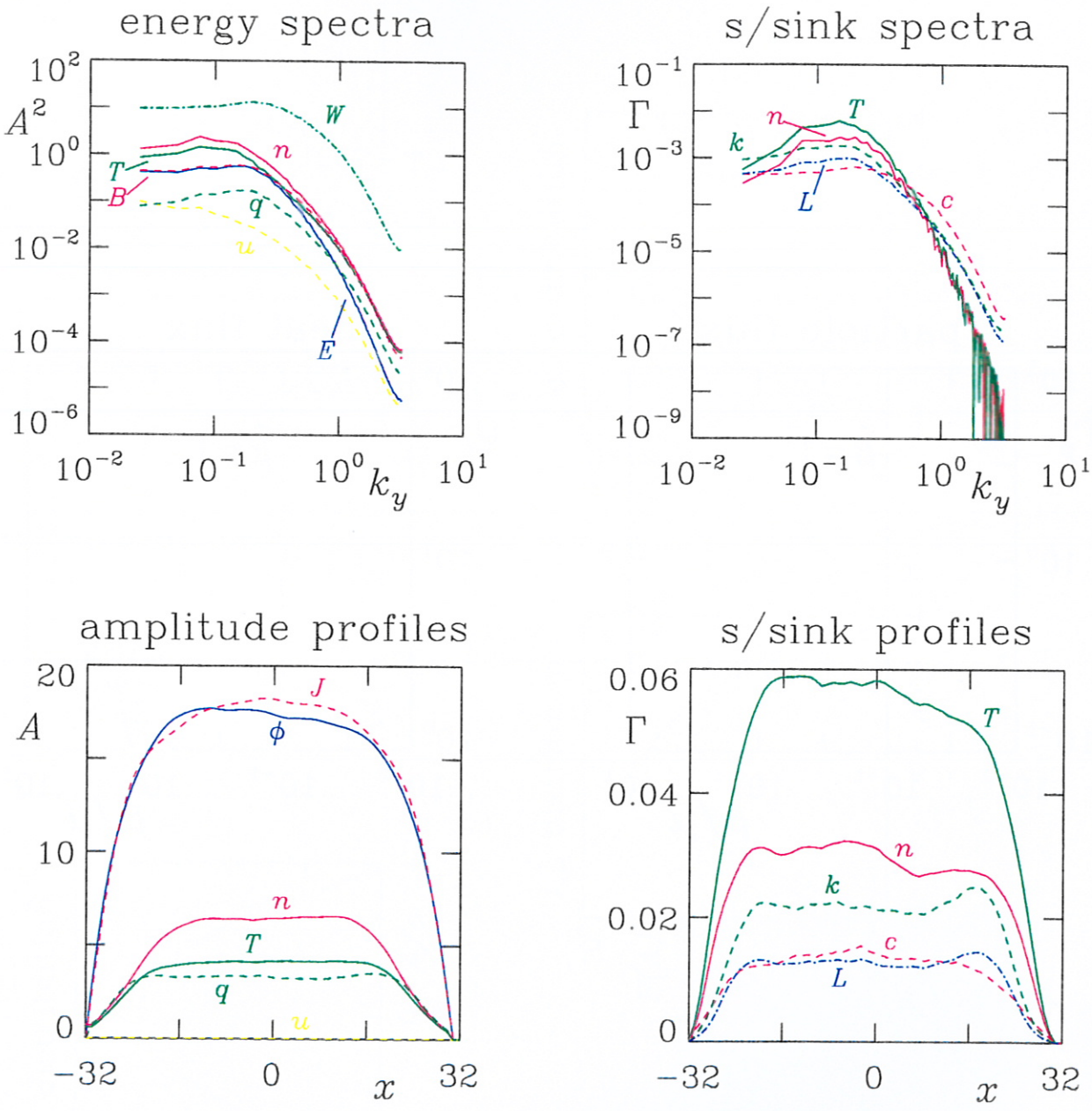
energy spectra
10^2
A^2
10^0
10^{-2}
10^{-4}
10^{-6}
10^{-2}
10^{-1}
10^0
k_y
10^1
W
n
T
B
q
u
E
s/sink spectra
10^{-1}
Γ
10^{-3}
10^{-5}
10^{-7}
10^{-9}
n
T
k
L
c
10^{-2}
10^{-1}
10^0
k_y
10^1
amplitude profiles
20
A
10
0
J
ϕ
n
T
q
u
−32
0
x
32
s/sink profiles
0.06
Γ
0.04
0.02
0
T
n
k
c
L
−32
0
x
32

Fig 2

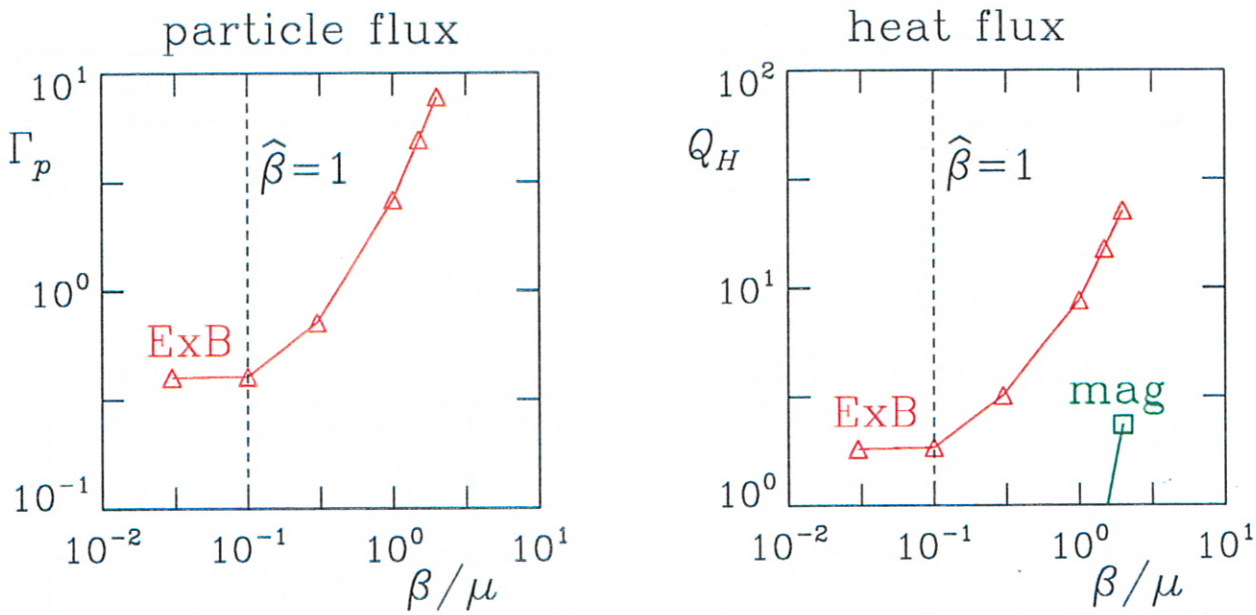
particle flux
Γ_p
10^1
10^0
10^{-1}
$\widehat{\beta}=1$
ExB
10^{-2}
10^{-1}
10^0
10^1
β/μ
heat flux
Q_H
10^2
10^1
10^0
$\widehat{\beta}=1$
ExB
mag
10^{-2}
10^{-1}
10^0
10^1
β/μ

Fig. 3

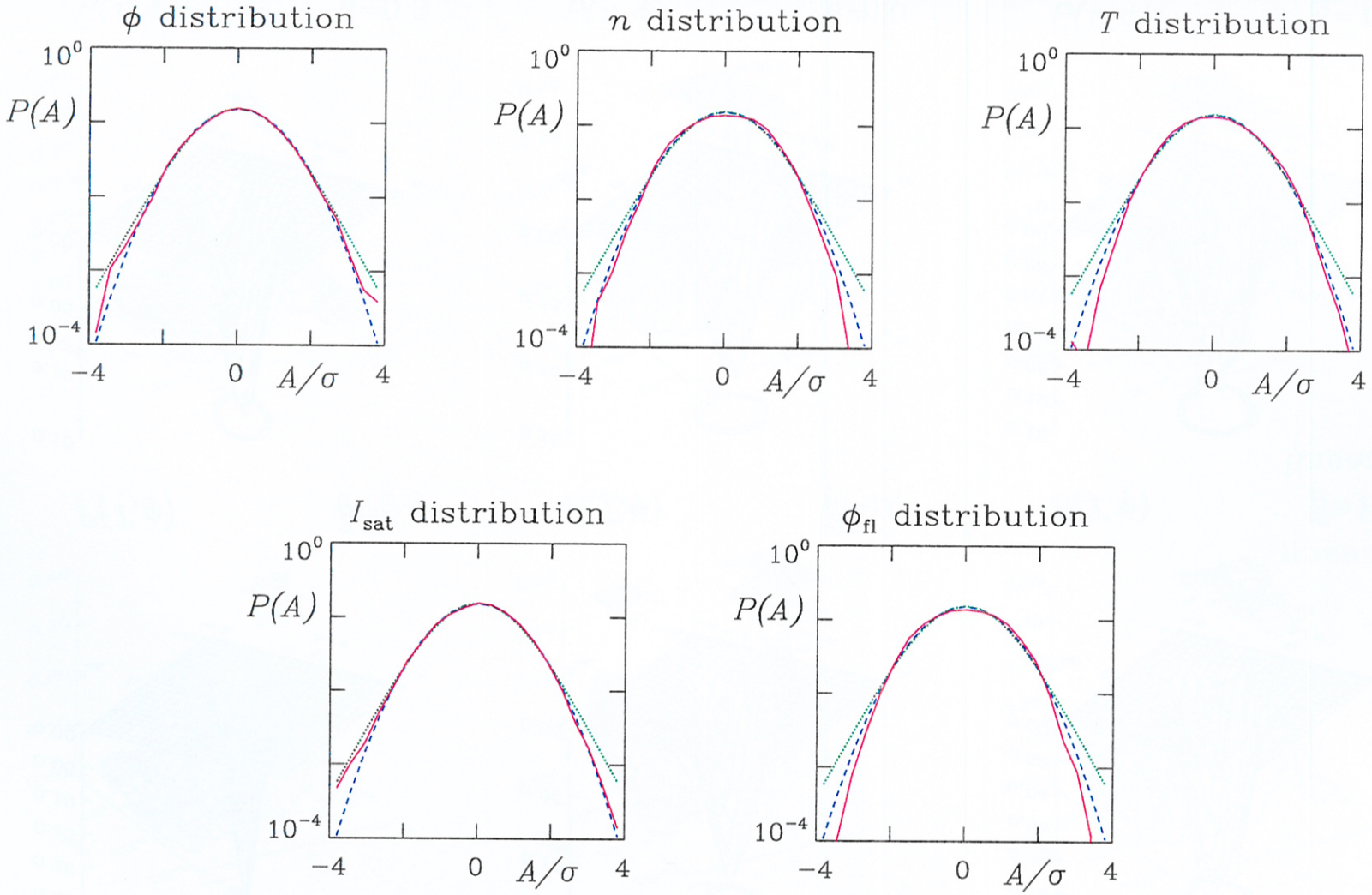
ϕ distribution
n distribution
T distribution
I_{sat} distribution
ϕ_{fl} distribution
10^0
10^{-4}
$P(A)$
-4
0
A/σ
4

Fig 4

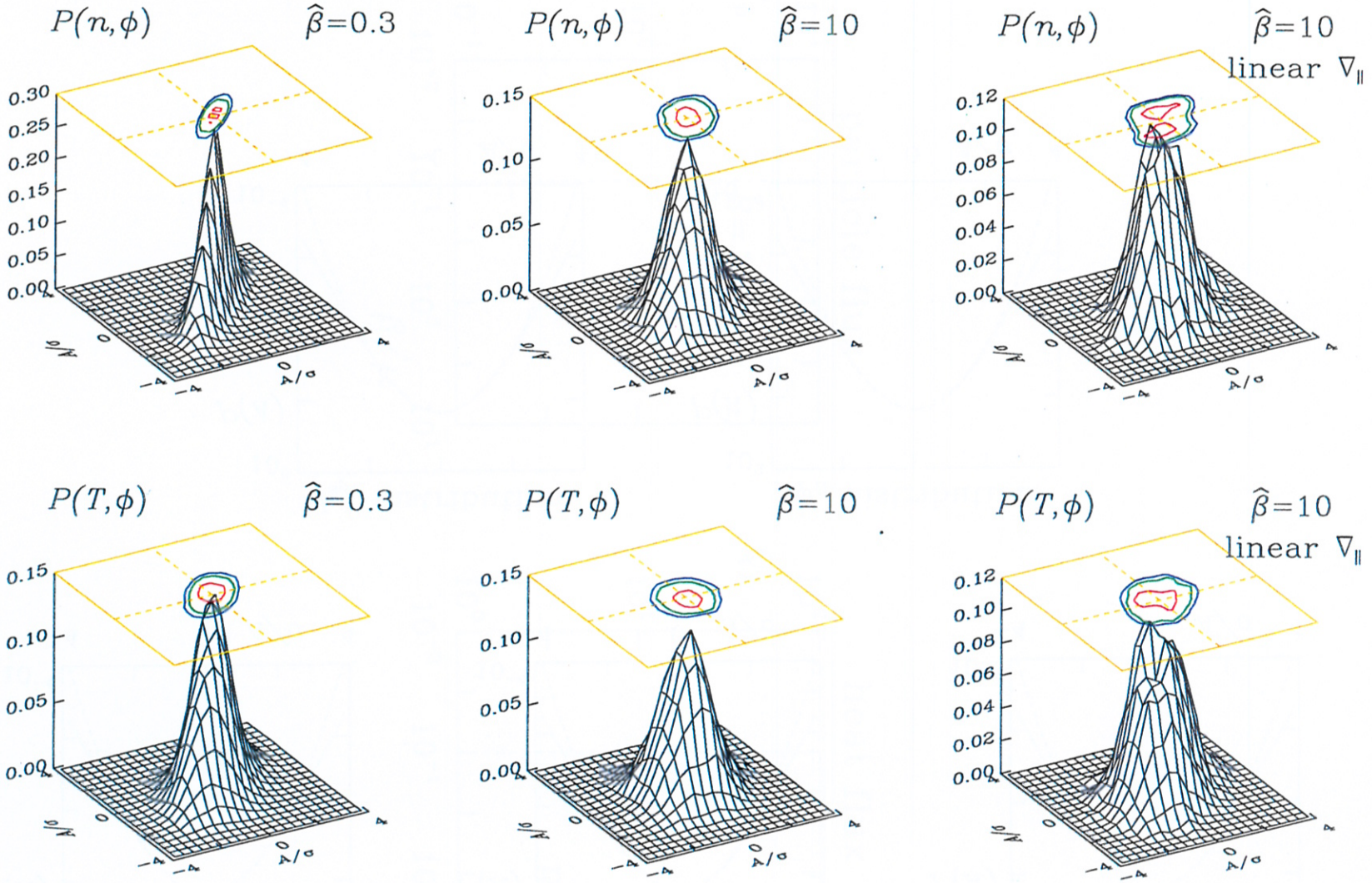
$P(n,\phi)$
$\widehat{\beta}=0.3$
$P(n,\phi)$
$\widehat{\beta}=10$
$P(n,\phi)$
$\widehat{\beta}=10$
linear $\nabla_{\parallel}$
$P(T,\phi)$
$\widehat{\beta}=0.3$
$P(T,\phi)$
$\widehat{\beta}=10$
$P(T,\phi)$
$\widehat{\beta}=10$
linear $\nabla_{\parallel}$

Fig 5

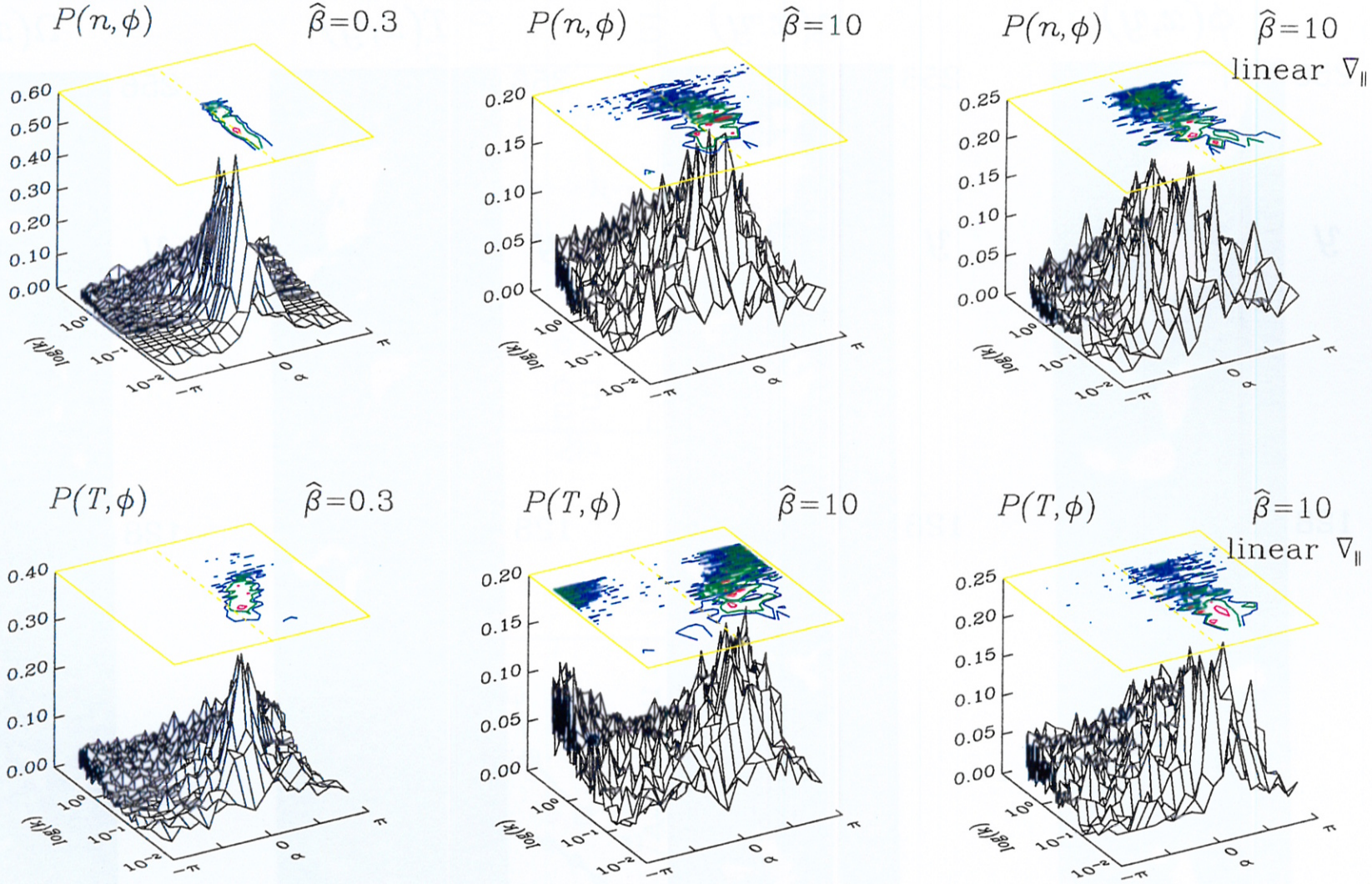
$P(n,\phi)$
$\widehat{\beta}=0.3$
$P(n,\phi)$
$\widehat{\beta}=10$
$P(n,\phi)$
$\widehat{\beta}=10$
linear $\nabla_{\|}$
$P(T,\phi)$
$\widehat{\beta}=0.3$
$P(T,\phi)$
$\widehat{\beta}=10$
$P(T,\phi)$
$\widehat{\beta}=10$
linear $\nabla_{\|}$
log(κ)
φ

Fig 6

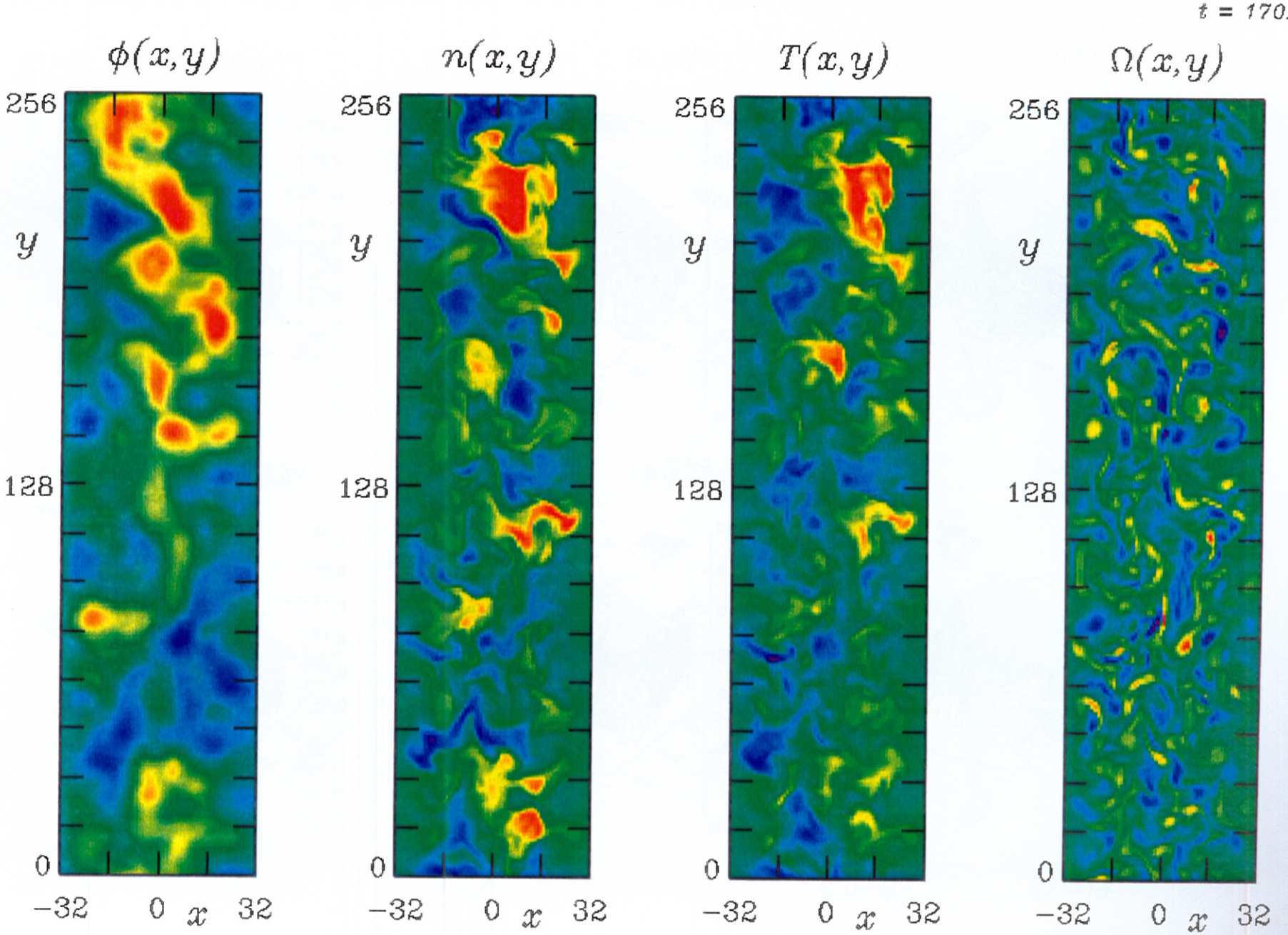

Fig 7

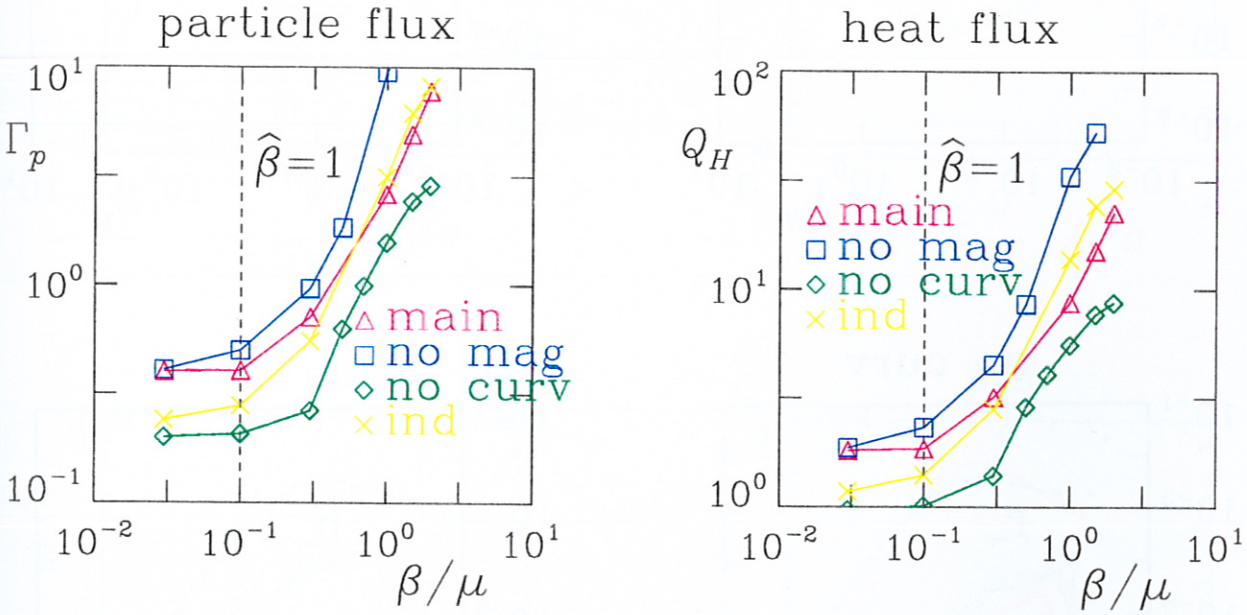
particle flux
heat flux
Γ_p
Q_H
$\widehat{\beta}=1$
main
no mag
no curv
ind
10^{1}
10^{0}
10^{-1}
10^{2}
10^{-2}
β/μ

Fig 8

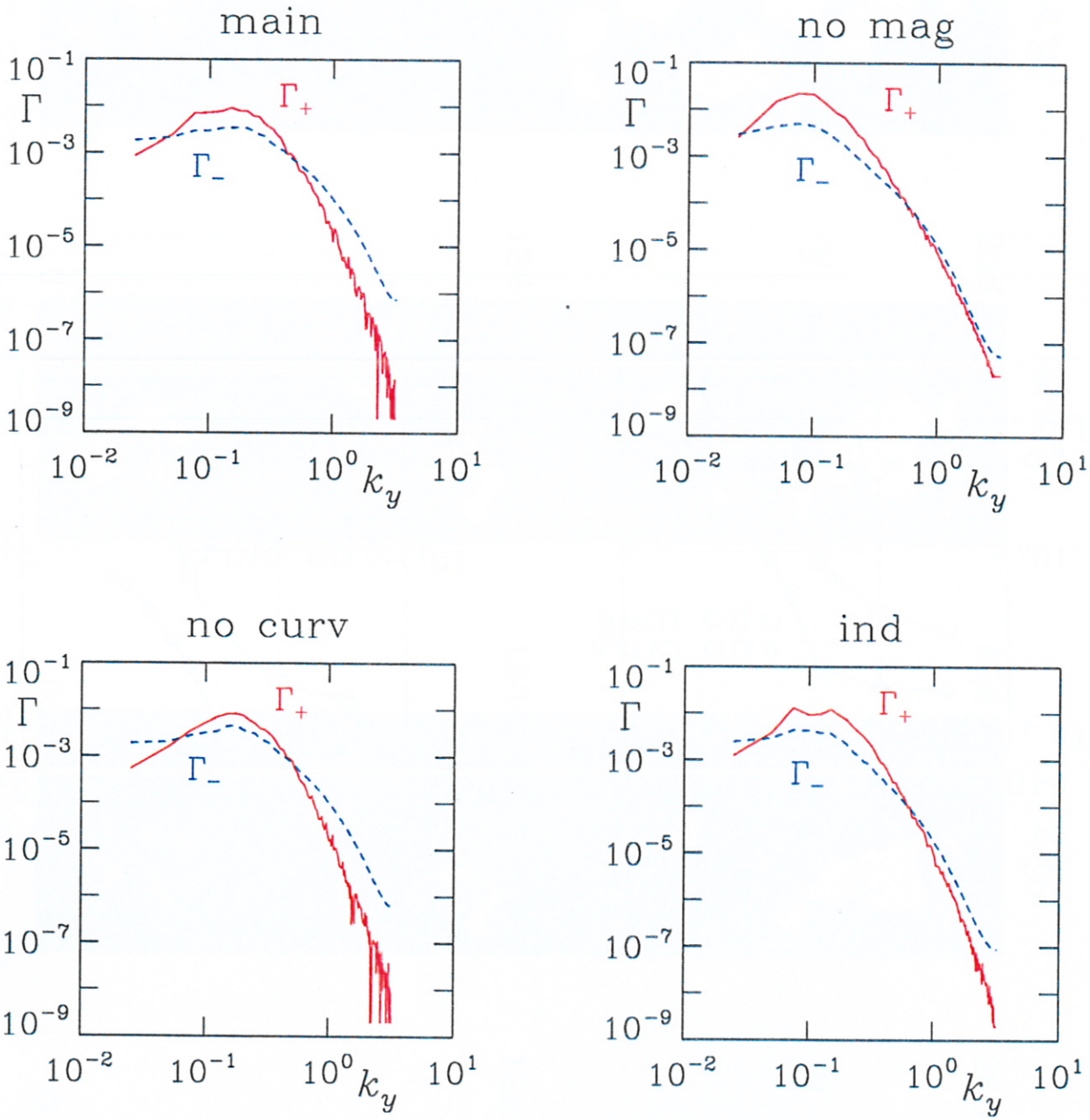
main
no mag
no curv
ind
10^{-1}
Γ
10^{-3}
10^{-5}
10^{-7}
10^{-9}
Γ_+
Γ_-
10^{-2}
10^{-1}
10^{0}
k_y
10^{1}

Fig 9

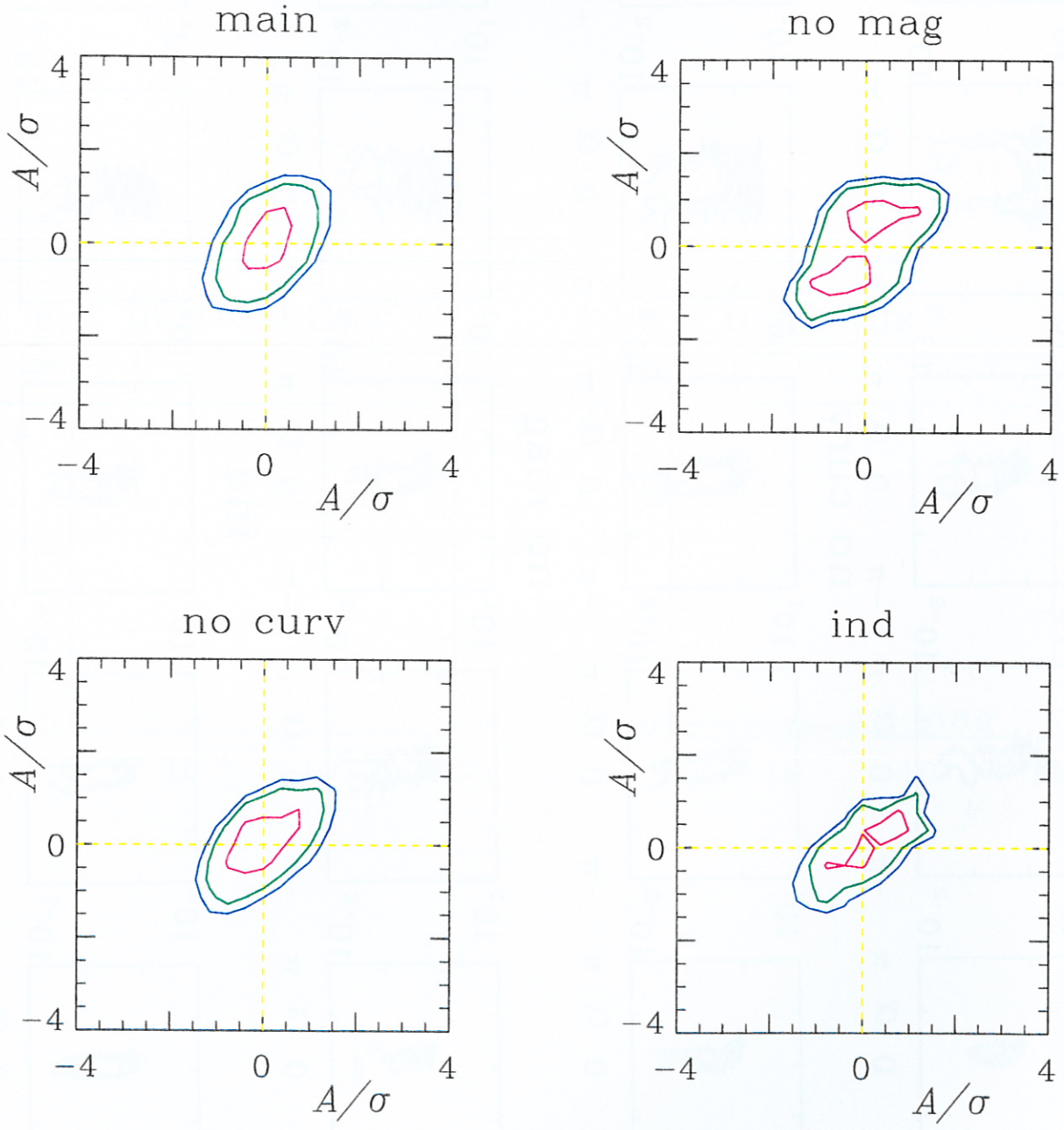

Fig 10

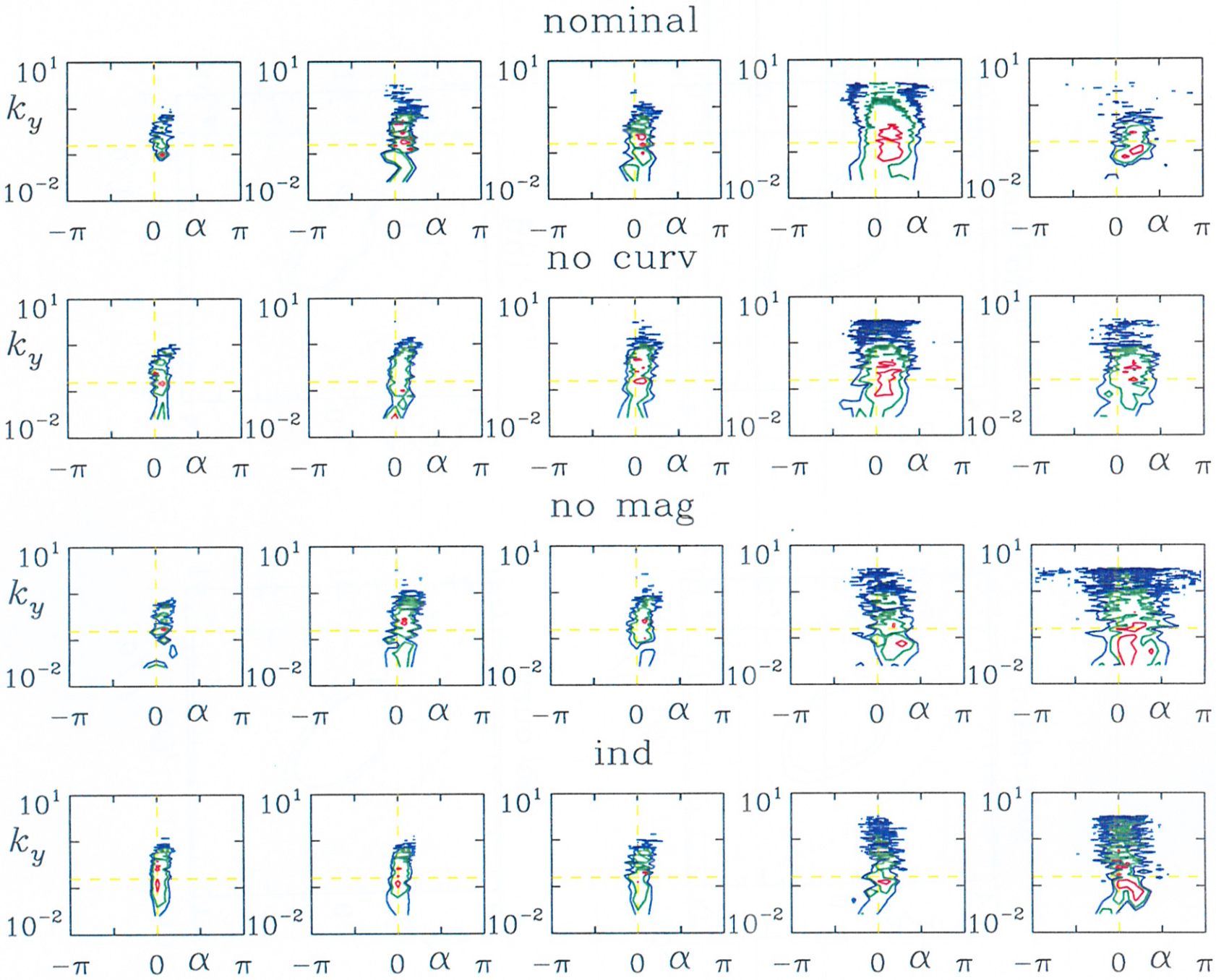

Fig 11

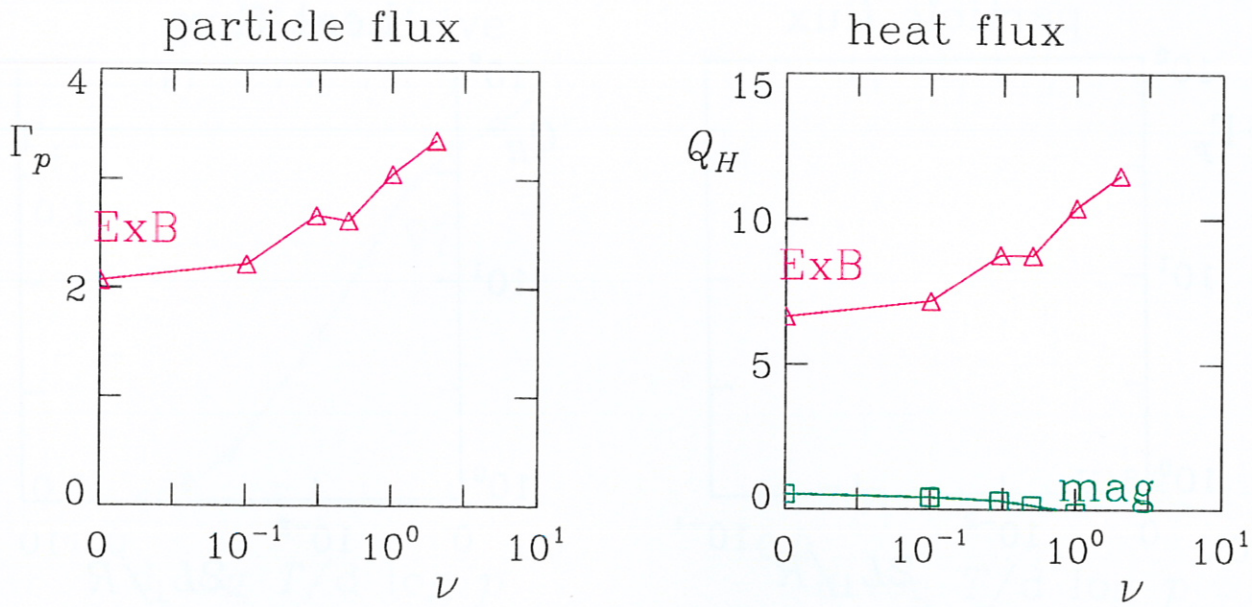
particle flux
Γ_p
4
2
0
ExB
0
10^{-1}
10^{0}
10^{1}
ν
heat flux
Q_H
15
10
5
0
ExB
mag
0
10^{-1}
10^{0}
10^{1}
ν

Fig 12

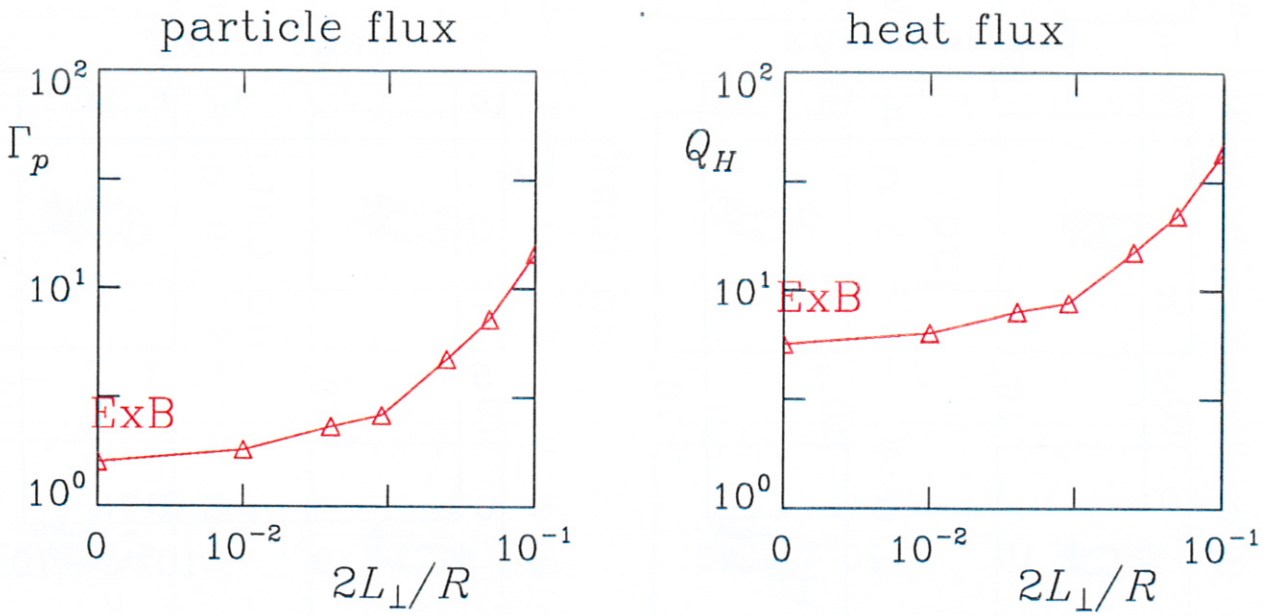
particle flux
10^2
Γ_p
10^1
ExB
10^0
0
10^{-2}
10^{-1}
$2L_\perp/R$
heat flux
10^2
Q_H
10^1
ExB
10^0
0
10^{-2}
10^{-1}
$2L_\perp/R$

Fig 13

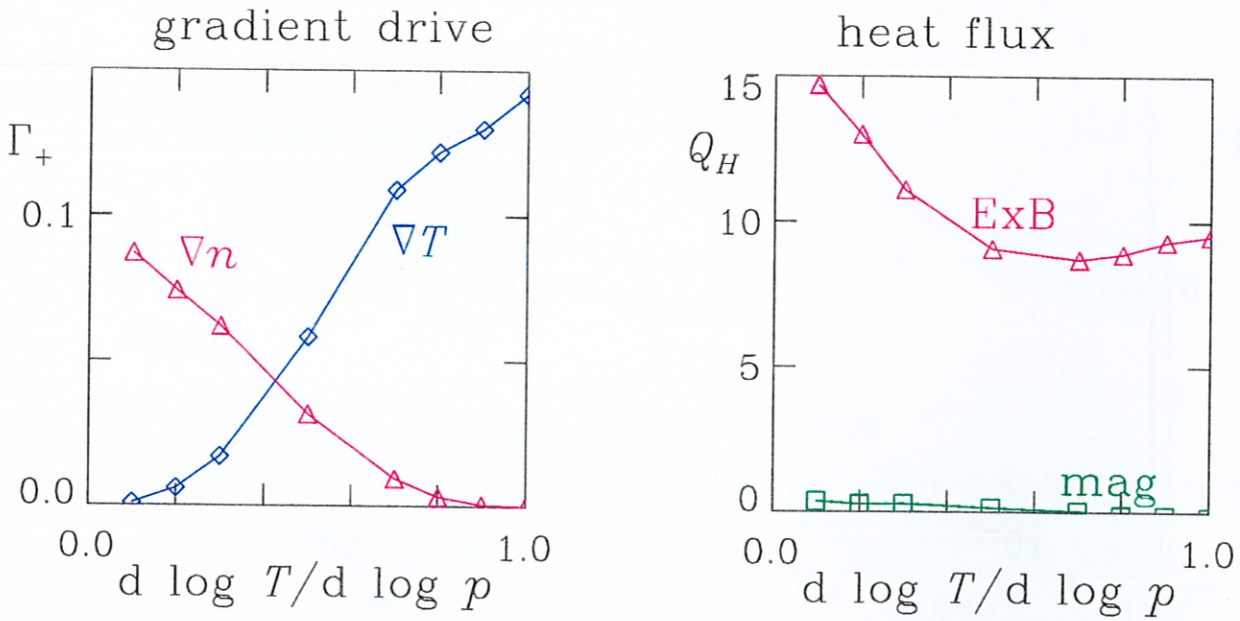
gradient drive
Γ_+
0.1
0.0
∇n
∇T
0.0
1.0
d log T/d log p
heat flux
15
Q_H
10
5
0
ExB
mag
0.0
1.0
d log T/d log p

Fig 14

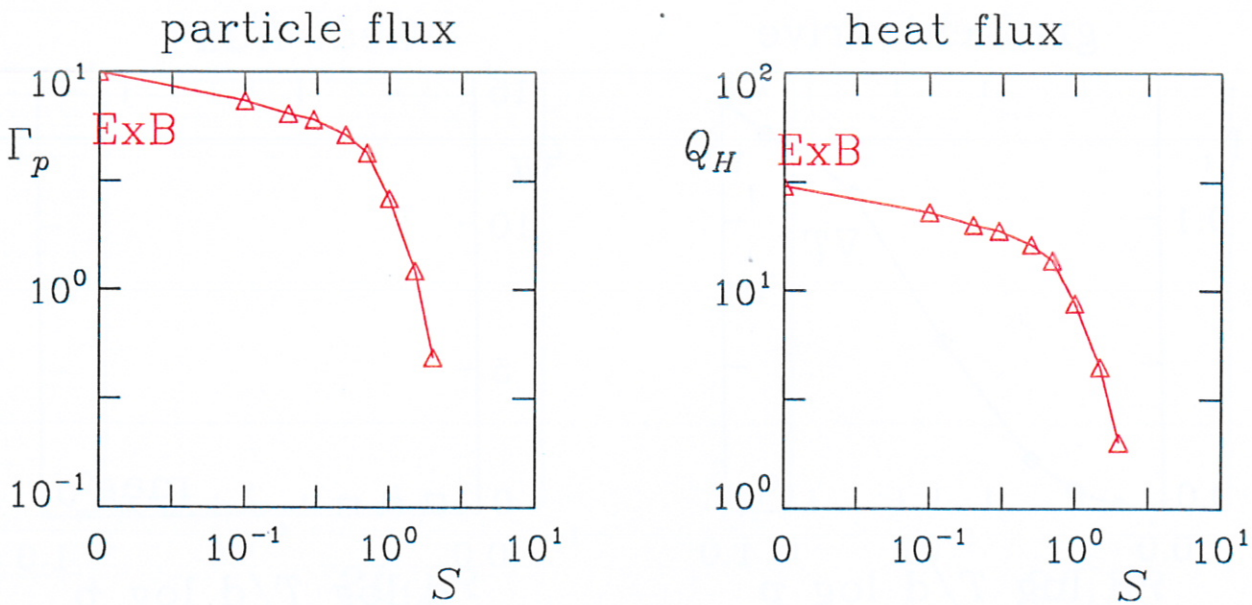
particle flux
10^1
Γ_p
ExB
10^0
10^{-1}
0
10^{-1}
10^0
10^1
S
heat flux
10^2
Q_H
ExB
10^1
10^0
0
10^{-1}
10^0
10^1
S

Fig 15

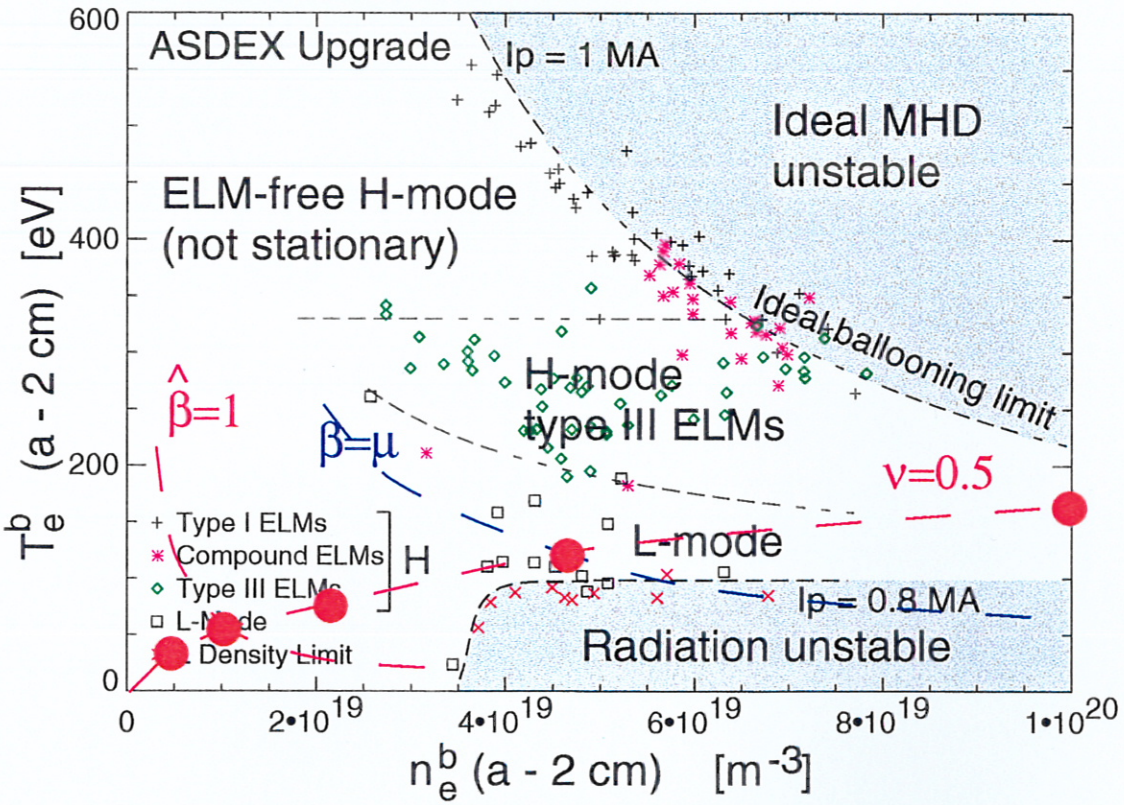
ASDEX Upgrade
Ip = 1 MA
Ideal MHD
unstable
ELM-free H-mode
(not stationary)
Ideal ballooning limit
H-mode
type III ELMs
β=1
β=μ
ν=0.5
L-mode
Ip = 0.8 MA
Radiation unstable
Type I ELMs
Compound ELMs
Type III ELMs
L-Mode
Density Limit
H
600
400
200
0
0
2•10^19
4•10^19
6•10^19
8•10^19
1•10^20
T_e^b (a - 2 cm) [eV]
n_e^b (a - 2 cm) [m^-3]

Fig 16